ABSTRACT

Title of Document: MOLECULAR DYNAMICS SIMULATION OF DICARBOXYLIC ACID COATED AQUEOUS AEROSOL: STRUCTURE AND PROCESSING OF WATER VAPOR

Xiaofei Ma, M.S., 2010

Directed By: Professor Michael R. Zachariah, Department of Mechanical Engineering

Low molecular weight dicarboxylic acids constitute a significant fraction of water-soluble organic aerosols in the atmosphere. They have a potential contribution to the formation of cloud condensation nuclei (CCN) and are involved in a series of chemical reactions occurring in atmosphere. In this work, molecular dynamics simulation method was used to probe the structure and the interfacial properties of the dicarboxylic acid coated aqueous aerosol. Low molecular weight dicarboxylic acids of various chain lengths and water solubility were chosen to coat a water droplet consisting of 2440 water molecules. For malonic acid coated aerosol, the surface acid molecules dissolved into the water core and form an ordered structure due to the hydrophobic interactions. For other nanoaerosols coated with low solubility acids, phase separation between water and acid molecules was observed. To study the water processing of the coated aerosols, the water vapor accommodation factors were calculated.

MOLECULAR DYNAMICS SIMULATION OF DICARBOXYLIC ACID COATED AQUEOUS AEROSOL: STRUCTURE AND PROCESSING OF WATER VAPOR

By

Xiaofei Ma

Thesis submitted to the Faculty of the Graduate School of the
University of Maryland, College Park, in partial fulfillment
of the requirements for the degree of
Master of Science
2010

Advisory Committee:
Professor Michael R. Zachariah, Chair
Professor Tobias von Petersdorff
Professor George W. Mulholland

Dedication

To

My parents

Yucheng Ma and Xiaoling Liang,

And my wife

Yun Zhou.

Thank you for your unconditional love and support. Thank you for your unwavering faith and absolute belief in my abilities. You have sacrificed so much and waited so long for this moment to come true and I dedicate this thesis to you.

Acknowledgements

First and foremost, I thank my thesis advisor, Professor Michael R. Zachariah, for his generous support and guiding me during my Master research. Without his invaluable ideas, experience and strategic insights this thesis would not have been possible.

I would like to thank Professor George W. Mulholland and Professor Tobias von Petersdorff for serving on my committee and taking time editing my thesis, attending my defense.

I would like to thank Dr. Purnendu Chakraborty for teaching me and helping me get started with Molecular Dynamics and Dr. Brian J. Henz for helping me solving parallel computing problems. I would also like to give a special thanks to my friend Dr. Lei Zhou and group members who have made this journey thoroughly enjoyable.

Table of Contents

List of Tables

List of Figures

Chapter 1: Introduction

Organic material is ubiquitous in the earth's atmosphere and represents an important fraction of the fine aerosol mass. Studies have shown that total organic carbon can represent 10-65% of the aerosol mass and exists as a complex mixture of hundreds of organic compounds, while define secondary organic carbon can contribute up to 25-50% of fine aerosol mass in urban polluted areas[1]. Indirectly, atmospheric aerosols can affect the radiative properties and lifetime of clouds and thus have an influence on global climate by acting as cloud condensation nuclei (CCN)[2]. Observations have revealed that more than 60% of the CCN can consist of organic constituents[3]. Recent experimental studies and thermodynamic analysis of organic marine aerosols even suggest that atmospheric aerosols could act as pre-biotic chemical reactors and play a role in the origin of life[4, 5]. Despite the considerable fraction of organic matters in atmosphere aerosol and significant importance of their environmental and biological functions, little is known about their structure and influence on atmospheric processes.

The organic material can be water-soluble and insoluble, volatile and nonvolatile, surface-active and surface-inactive, biogenic and anthropogenic. Depending on their physical properties, the organics can form different structured films on the existing aerosol particle surfaces. Water-insoluble organic molecules are likely to be closed-packed and oriented and thus tend to form "condensed films" on the particle surfaces. Phase transitions which correspond to differing degrees of ordering of the surfactant

molecules can take place in those films[6]. Our previous molecular dynamic simulation results[7] on the structure of long-chain fatty acid coated nanoaerosols showed that in the final stage of equilibrium, the fatty acid molecules can reside into a "solid" phase with the hydrocarbon tails all aligned together pointing out of the aerosol and the hydrophilic headgroups are close packed on the aerosol surface. On the other hand, water-soluble organic surfactant molecules tend to form less compact films which do not undergo phase transitions to more compact structures. Not long ago, a conceptual "inverted micelle" model[8] has been proposed for the structure, composition and atmospheric processing of organic aerosols. In this model, an aqueous core is encapsulated in an inert, hydrophobic organic monolayer. The organic molecules lie with their polar heads inserted into the ionic aqueous core and their hydrophobic hydrocarbon tails exposed to the atmosphere. In our previous simulation work of the structure of long-chain fatty acid coated nanoaerosols[9], we observed that the coated particles indeed favor the "inverted micelle" structure and this monolayer has an influence on the water processing of the nanoaerosols.

The accommodation of water vapor to the aerosol surface is a critical atmospheric process, playing an important role in the growth of cloud condensation nuclei into cloud droplets and is strongly affected by the composition, structure and surface properties of the aerosol. Due to the presence of the organic films, transfer of gas species into the aerosol could be impeded, evaporation could be slowed and the heat transfer could be influenced. To complicate this already difficult problem, atmospheric "processing" of the film compounds by atmospheric oxidants would even alter the surface properties of the aerosol, thus, could lead to the change of its

reactivity[6, 8]. Thus, more studies have focused on the influence of this organic film on the atmospheric processing.

Among various kinds of organic compounds, low molecular weight dicarboxylic acids have attracted much attention due to their large prevalence and unique physicochemical properties. This type of acids has been identified as one of the major organics in both urban and rural areas and are ubiquitous organic aerosol constituent in the marine and even Arctic atmosphere[10, 11]. Observations have showed that dicarboxylic acids are also commonly found in the organic fraction of secondary aerosols. However, their formation and partition to the aerosol phase are still unclear. In biology, dicarboxylic acids are important metabolic products of fatty acids. During recent years, a considerable effort has been made to understand the properties of low molecular weight dicarboxylic acids (C3-C9). It is known that the physicochemical properties of low molecular weight dicarboxylic acids such as solubility, vapor pressure, evaporation rate, melting and boiling points alternate with the number of carbon atoms[12, 13]. Those physicochemical properties have profound effect on the CCN activity. One of the major questions surrounding organic compounds as CCN focuses on the changes in surface tension of the droplet due to the presence of the organic and the solubility of the compound[2]. Water-soluble matters are known to affect droplet activation by lowering the surface tension and thus changing the critical drop radius. Experiments have confirmed that this effect can be well predicted by Kohler theory for soluble inorganic species and organics that are wettable by water[14]. However, when considering extending the current theory, low-solubility organic species are equally important. The low molecular weight dicarboxylic acids (C3-C9)

cover a wide range of solubility and thus provide an excellent platform to study the effect of solubility on the CCN activation.

With hydrophilic groups at both ends of a hydrophobic hydrocarbon chain, dicarboxylic acids are bolaamphiphilic molecules. The strucutre and phase behavior of these molecules in a particular type of medium are determined by unique intermolecular interations: the hydrophobic interactions between hydrocarbon chains, the hydrophilic and/or the electrostatic interactions between the head groups. When amphiphlic molecules are dispersed in water, the hydrophobic interations of the hydrocarbon chains drive the molecules to self-assemble into structures where the hydrophobic tails are shielded from unfavorable interactions with water by the hydrophilic, polar head groups[15]. Like amphiphilic molecules, bolaamphiphilic molecule aggregates driven by hydrophobic interactions can form rich self-assembly strucutres, such as spherical lipid particles made of monolayer lipid membranes, vesicles produced by long-chain molecules, and micelles from short-chain, water-soluble bolaamphiphiles[16]. Compared with amphilic molecules, the introduction of a second hydrophilic head group generally induces a higher solubility in water and an increase in the critical micelle concentration.

Previous experiments have been carried out to investigate the cloud activity of various pure dicarboxylic acid aerosols from highly-soluble acids to almost insoluble acids[10, 14, 17]. TDMA (Tandem DMA) method is frequently used in the laboratory studies. In this method, the first DMA produces nearly monodisperse particles of a known size while the second DMA measures the particle size distribution of final aerosol. However, there are some drawbacks associated with this method. First, the

DMAs are designed for classifying spherical particles, and the results are interpreted based on singly charged assumption. Therefore, depending on particle morphology, mass and cross-sectional area which affects the charging efficiency, there is a possibility that DMA could lead to incorrect size classification. Second, the ion-mobility method deals with the whole aerosol population, so it is impossible to use this method to monitor the water processing of individual particles. In fact, since molecular-processes involve dynamics happening over short distances (nanometer length scale) and short times (nanoseconds time scale), these processes are difficult to probe experimentally. Furthermore, the atmospheric organic aerosols usually consist of more than one chemical species and the organics can form complicate structures such as monolayers, thin films on the aerosol surfaces. It is an experimental challenge to create reproducible, well-characterized aqueous aerosol particles which are coated with an organic film. However, on the other hand, the structure of complex aerosols can be explicitly defined in molecular simulations and the dynamics of molecular-scale process can be followed explicitly as well.

In this work, we employed molecular dynamic simulation method to study the structure evolution and water processing of various dicarboxylic acids coated water droplets. Two questions are addressed in our study: 1. what is the relationship between the aerosol final structure and physical properties of coated dicarboxylic acid molecules? 2. How does the aerosol structure affect the water processing of the coated aerosol?

The dicarboxylic acids simulated in this study were malonic acid (C3), succinic acid (C4), glutaric acid (C5), adipic acid (C6), pimelic acid (C7), suberic acid (C8),

azelaic acid (C9) and branched azelaic acid (C9b). The physical properties of these dicarboxylic acids are summarized in Table 1.1.

Dicarboxylic Acid	**Chemical Formula**	**Molar Mass (g/mol)**	**Density (g/cm^3)[2, 10, 13]**	**Solubility in Water (g per 100 g water)[2, 10]**
malonic acid (C3)	HOOC-(CH_2)-COOH	104.06	1.631	161
succinic acid (C4)	HOOC-(CH_2)$_2$-COOH	118.09	1.572	8.8
glutaric acid (C5)	HOOC-(CH_2)$_3$-COOH	132.12	1.424	116
adipic acid (C6)	HOOC-(CH_2)$_4$-COOH	146.14	1.360	2.5
pimelic acid (C7)	HOOC-(CH_2)$_5$-COOH	160.17	1.281	71
suberic acid (C8)	HOOC-(CH_2)$_6$-COOH	174.20	1.272	0
azelaic acid (C9)	HOOC-(CH_2)$_7$-COOH	188.22	1.251	0

Table 1.1. Physical properties of the dicarboxylic acids studied in this work

Chapter 2: Molecular Dynamics Simulation

2.1. Introduction

The molecular dynamic modeling problem can be divided into two tasks[18]: developing a suitable model for the problem and performing molecular dynamics simulations using that model. The model developing consists of three parts: 1) modeling the interactions among the molecules 2) modeling the interactions between the system and the environment 3) developing the equations governing the molecular motions. The model for molecular interactions is contained in an intermolecular potential energy function, which is usually a sum of isolated pair interactions. The details of the intermolecular forces field used in this study are reviewed in section 2.2. The second part of the model developing encompasses boundary conditions which describe the interactions between the molecules with their surroundings. Section 2.3 gives an overview of the boundary conditions used in this study. The third part of the simulated model encompasses classic dynamics which give the equation of motion for the molecules. The basics of Newtonian dynamics are described in section 2.4. Performing molecular dynamics simulation using the developed models consists of two parts: 1) generating molecular trajectories and 2) analyzing the trajectories. Generating molecular trajectories involves integrating the equation of motion. The numerical algorithm for solving differential equations is finite difference method. The details of trajectory generating are discussed in section 2.5. The final step in molecular dynamic simulation is analyzing the molecular trajectories. Physical properties of the system can be calculated at this step. The detailed computation

procedures are discussed in section 2.6. The hierarchy of the principal steps in molecular dynamic modeling is presented in Figure 2.1.

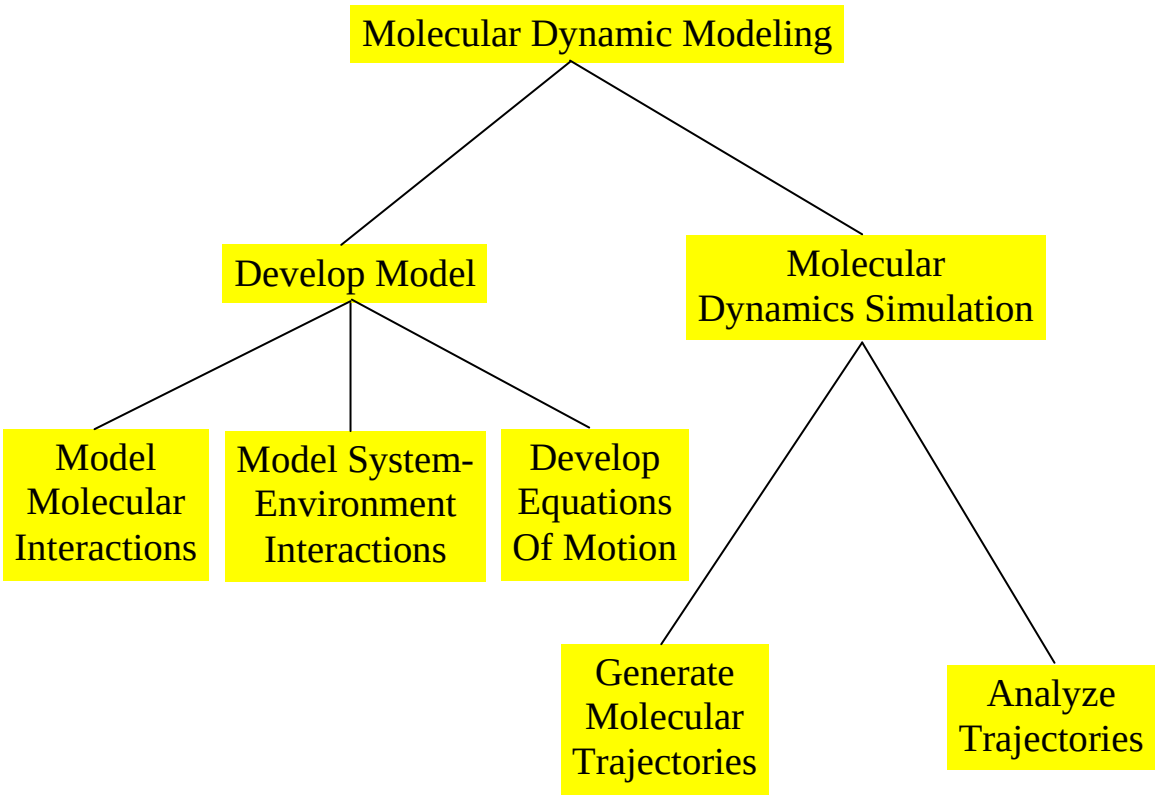

Figure 2.1. Hierarchy of the principal steps in molecular dynamic modeling[18]

2.2. Intermolecular Force Field

The molecular system we investigate is too large to be considered by quantum mechanics. Force field method, on the other hand, ignores the electronic motions within an atom and calculates the total energy of a system as a function of system configurations. The basic assumption behind the force field method is the Born-

Oppenheimer approximation which separates the motion of the electrons in a molecule from the motion of the nuclei based on the fact that the nuclear motion is much slower than the electron motion. Force fields are empirical and are designed to reproduce structural properties. When used properly, force field method can produce answers that are as accurate as quantum mechanical calculation in a fraction of the computer time. However, computations using force field method can not provide properties dependent on the electronic distribution within a molecule[19].

The molecular force field usually contains terms that describe the bond stretching, angle bending, dihedral interactions, improper interactions (The improper term ensures the maintenance of planarity at sp^2 hybridized atoms and the configuration at chiral centers) and non-bonded interactions. Both the functional form and the parameters should be specified in order to define a force field. The force fields used in this work are reviewed below.

2.2.1. Force Field for Simulation of Water

Despite its small size, water is one of the most challenging systems to model accurately. A wide range of water models have been proposed which can fall into three types[19]. Simple interaction-site models use three and five interaction sites and maintain each water molecule in a rigid geometry. The simple models can provide very good results in reasonable computation time for many properties of liquid water such as density, enthalpy of vaporization, heat capacity and diffusion coefficient. A flexible water molecule model permits internal changes of the molecule and can be used to calculate the vibrational spectrum. Polarizable water models include the

many-body effects and polarization effects and are suitable for modeling inhomogeneous systems.

In this study, we used one of the simple water models, the extended simple point charge (SPC/E) interaction potential developed by Berendsen *et al*[20, 21]. It's an updated version of the SPC model. This model consists of a total of three sites for the electrostatic interactions of water with OH distance of 0.1nm and HOH angle of 109.47 degrees. The partial positive charges of +0.4328e on the hydrogen atoms are exactly balanced by the partial negative charges of -0.8476e located on the oxygen atom. A pairwise Lennard-Jones interaction centered on the oxygen atoms is used to compute the van der Waals forces between two water molecules. The expression is given by:

$$V_{LJ}(r_{ij}) = -(\frac{A}{r_{ij}})^6 + (\frac{B}{r_{ij}})^{12}$$

with A=0.37122(kJ/mol)$^{1/6}$nm, B=0.3428(kJ/mol)$^{1/12}$nm, where r_{ij} is the distance between two oxygen atoms. The SPC/E potential has been studied extensively. It can provide accurate reproduction of water surface tension and its temperature dependence[22]. The effects of simulation size and the treatment of long-range interactions on surface tension have been shown to be less than 10%. A comparison of SPC/E model with other simple models is given in Table 2.1.

	SPC/E	SPC	TIP3P	BF	TIP4P	ST2
Distance between OH, A	1.0	1.0	0.9572	0.96	0.9572	1.0

Angle HOH, deg	109.47	109.47	104.52	105.7	104.52	109.47
$A \times 10^{-3}$, kcal A^{12}/mol	629.4	629.4	582.0	560.4	600.0	238.7
Specific heat C, kcal A^6/mol	625.5	625.5	595.0	837.0	610.0	268.9
Charge on O	-0.8472	-0.82	-0.834	0.0	0.0	0.0
Charge on H	0.4238	0.41	0.417	0.49	0.52	0.2375
Charge on M	0.0	0.0	0.0	-0.98	-1.04	-0.2375
Distance between OM, A	0.0	0.0	0.0	0.15	0.15	0.8

Table 2.1. Comparison of different simple water models[19]

2.2.2. Force Field for Simulation of Dicarboxylic Acid Molecule

For modeling the dicarboxylic acid molecules, we used a mixture of "fully atomistic" and "united atom" methods. The high-accuracy/high computational requirement fully atomistic method is used to model the carboxyl group (-COOH group) while the less accurate/lower computational requirement united atom method is employed to simulate the methylene group (-CH_2 group). In the united atom setup, the number of interaction sites is reduced by subsuming some or all of the atoms into the atoms to which they are bonded. In a molecular simulation, the number of non-

bonded interactions scales with the square of the number of interaction sites present. Thus considerable computation savings are possible if the number of interaction site can be reduced. In our simulation, each methylene group (-CH_2 group) is represented by a single site with interactions defined between these sites. The van der Waals and electrostatic parameters are modified to take account of the adjoining hydrogen atoms. An example of the dicarboxylic acid studied in this work is shown in Figure 2.2. During the simulation, the O-H bond in the carboxyl group was kept rigid using SHAKE algorithm[23].

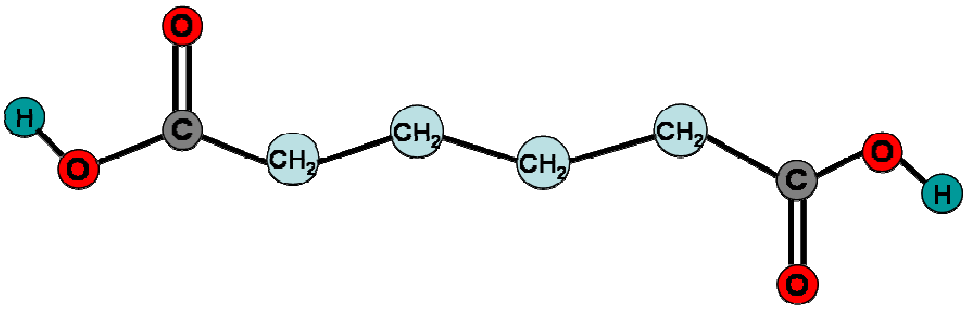

Figure 2.2. Structure of a dicarboxylic acid (C6)

The reliability of predictions from molecular simulations is determined largely by the accuracy of the representation of the intermolecular interaction potentials. The potentials used in our model include non-bonded interactions between each pair of atoms and bonded interactions between bonded atoms which have contributions from bond stretching, angle vibration, proper and improper dihedral interactions. The most time consuming part of a molecular dynamics simulation is the calculation of non-bonded energies and the corresponding forces. Fortunately, some forces fall off rapidly with distance. For example, at distance 2.5σ the Lennard-Jones potential has

just 1% of its value at σ. Thus, the most popular way to deal with the non-bonded interactions is to use a non-bonded cutoff. When a cutoff distance is employed, the interactions between all pairs of atoms that are further apart than the cutoff are set to zero. However, a cutoff distance introduces a discontinuity in both the potential energy and the force near the cutoff value, which breaks the conservation of energy[19]. One approach to counteract the discontinuity effects is to use a switching function. A switching function is a polynomial function of the distance by which the potential energy function is multiplied. In this study, we used the switched Lennard-Jones and the switched Coulombic potential with two cutoff distances to simulate the van der Waals interactions and the electrostatic interactions, respectively. The switched forces are given by:

$$E = \begin{cases} LJ(r) & r < r_{in} \\ S(r) \cdot LJ(r) & r_{in} < r < r_{out} \\ 0 & r > r_{out} \end{cases}$$

$$E = \begin{cases} C(r) & r < r_{in} \\ S(r) \cdot C(r) & r_{in} < r < r_{out} \\ 0 \quad r > r_{out} \quad / \end{cases}$$

$$LJ(r) = 4\varepsilon \left[\left(\frac{\sigma}{r} \right)^{12} - \left(\frac{\sigma}{r} \right)^{6} \right]$$

$$C(r) = \frac{C q_i q_j}{\varepsilon r}$$

$$S(r) = \frac{\left[{r_{out}}^2 - r^2 \right]^2 \left[{r_{out}}^2 + 2r^2 - 3{r_{in}}^2 \right]}{\left[{r_{out}}^2 - {r_{in}}^2 \right]^3}$$

Harmonic potentials of the form $E = K(x - x_0)^2$ (where K is a pre-factor, x is the position vector or angle and x_0 is the corresponding equilibrium value) were chosen to model bond stretching and angle vibrations. The equilibrium bond length and angle

are the values that are adopted in a minimum energy structure. The periodic function $E = K\left[1+\cos(n\phi - d)\right]$ was used to describe the proper dihedral interactions. For the improper interactions, harmonic potential $E = K(\chi - \chi_0)^2$ was chosen to keep a planar group in the same plane. The potential parameters used in the simulation were obtained from Gromacs force field database and listed in Table 2.2.

Atom	ε *(kcal/mol)*	$\sigma(\overset{o}{A})$
OW-OW	0.1553	3.166
HW1-HW1	0.0	0.0
HW2-HW2	0.0	0.0
HO-HO	0.0	0.0
OA-OA	0.2029	2.955
C-C	0.0970	3.361
O-O	0.4122	2.6260
CH2-CH2	0.1400	3.9647

Table 2.2.(a). Nonbonded Force Parameters

Bond	$K(kcal/mol/\overset{o}{A}^2)$	$r_0(\overset{o}{A})$
OW-HW1; OW-HW2	0.0	1.0
HO-OA	375.0	1.0
OA-C	450.0	1.36
C=O	600.0	1.23
C-CH2; CH2-CH2;	400.0	1.53

Table 2.2.(b). Harmonic Bond Parameters

Angle	$K(kcal/mol/rad^2)$	θ_0(deg)

HW1-OW-HW2	0.0	109.47
HO-OA-C	47.5	109.5
OA-C=O	60.0	124.0
OA-C-CH2	60.0	115.0
O=C-CH2	60.0	121.0
C-CH2-CH2; CH2-CH2-CH2	55.0	111.0

Table 2.2.(c). Harmonic Angle Parameters

Dihedral	*K(cal/mol)*	*n(integer)*	*d*(deg)
HO-OA-C-CH2; HO-OA-C=O	4.0	2	180
OA-C-CH2-CH2; O=C-CH2-CH2	0.1	6	0
C-CH2-CH2-CH2; CH2-CH2-CH2-CH2	1.4	3	0

Table 2.2.(d). Proper Dihedral Parameters

Improper Dihedral	$K(cal/mol/rad^2)$	χ_0(deg)
C OA CH2 O	40	0.0

Table 2.2.(e). Improper Dihedral Parameters

2.2.3. Non-bonded Neighbor List

The introduction of cutoff in non-bonded force calculations by itself may not dramatically reduce the computation time. This is due to the fact that we still need to calculate the distance between every pair of atoms in the system to decide whether they are close enough to have interactions. The calculation of the N(N-1) distances takes almost as much time as calculating the interaction energy itself.

Fortunately, in molecular dynamics simulation of fluid, an atom's neighbors do not change significantly during 10 to 20 time steps[18]. Thus, building a non-bonded neighbor list to store an atom's neighbor information is a good way to 'predict' each

atom's neighbors without having to calculate the distances between atoms in the system. The first of such neighbor list is due to Verlet 1967. A Verlet neighbor list stores the atoms within the cutoff distance together with the atoms that are slightly outside the cutoff distance. The structure of a Verlet neighbor list is presented in Figure 2.3. In brief, the Verlet neighbor list consists of a neighbor list array, L and a pointer array P. As shown in Figure 2.3., the pointer array indicates where in the neighbor list the first neighbor for a particular atom is located. Thus, the neighbors of atom I is stored in element L[P[i]] through L[P[i+1]-1] of the neighbor list array L. The neighbor list is updated at regular intervals throughout the simulation.

When the number of molecules in the system is large, a significant computational time is required just to update the neighbor list. Thus, an appropriate update frequency should be determined. Also, a correct skin distance which is the distance that neighbor list cutoff larger than the non-bonded cutoff should also be determined. There is a trade-off between the size of the cutoff and the frequency at which the neighbor list must be updated: the larger the skin distance, the less frequently the neighbor list has to be updated.

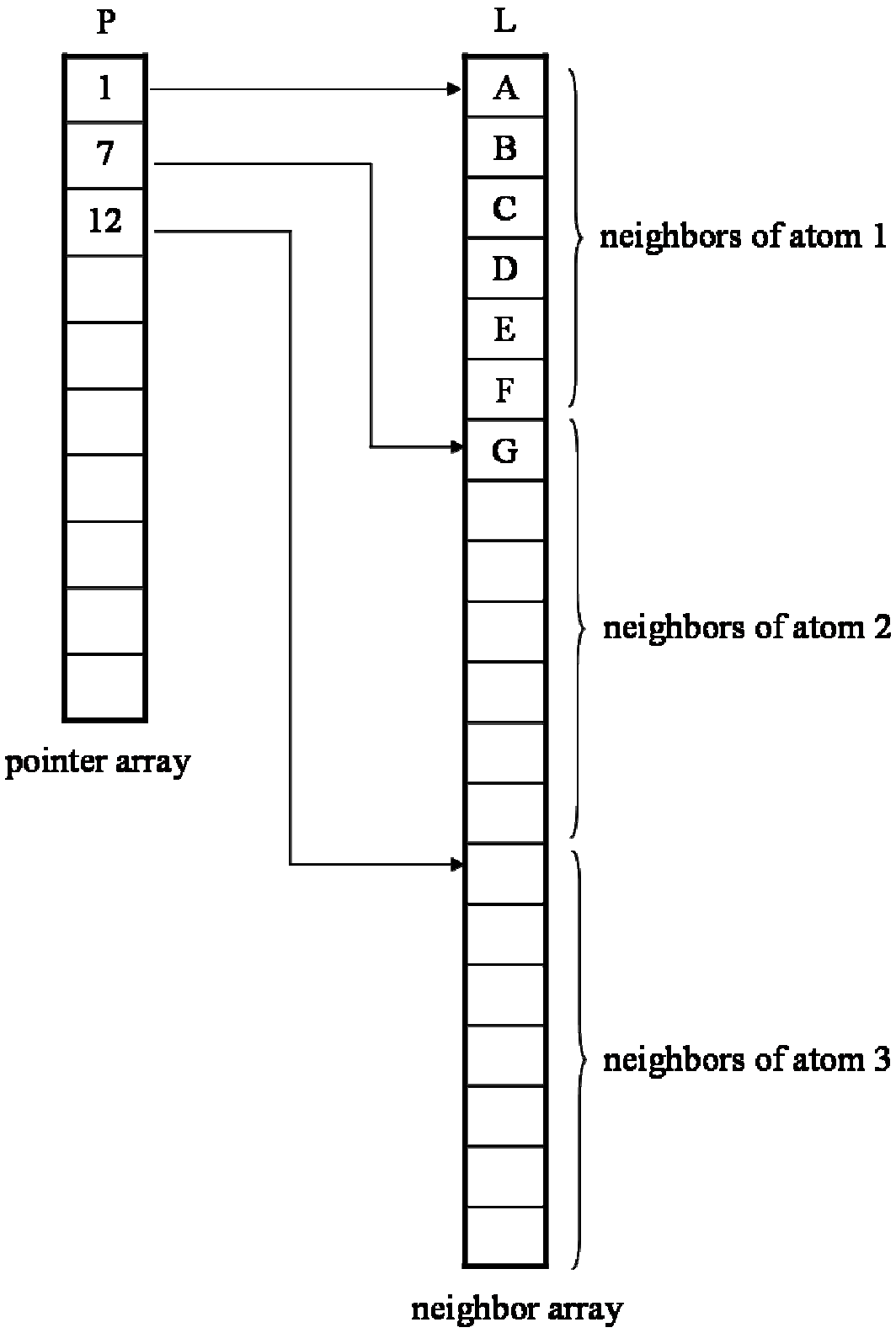

Figure 2.3. Non-bonded neighbor list

2.2.4. Long-range Forces Calculation: PPPM Method

The evaluation of Coulombic interactions which decay as r^{-1} for large system is a common computational problem. Various methods have been developed to handle long-range forces such as Ewald summation, the reaction field method, the fast multipole method (FMM), and the particle-particle particle-mesh (PPPM) method. In this work, the PPPM method is used to calculate the long-range forces.

The PPPM algorithms are a class of hybrid algorithms which combine the advantage of the PP (particle-particle) and PM (particle-mesh) methods[24]. The essence of the method is to express the inter-particle forces as the sum of two components: the short-range part and the smoothly varying part. The total short-range force on a particle is computed by particle-particle pair force summation and the smoothly varying part is approximated by the particle-mesh force calculation. The detailed mathematical derivation of this method is available in reference [24]. The basic steps in the PPPM method can be summarized as follows:

1. Compute the short ranged term
2. Form an effective density $W(r) = \sum_{i=1}^{N} W_i(r)$, where the specific forms for various $W_i(r)$ are given in reference [17].
3. Using the modified Coulomb Green's function to solve Poisson's equation to get the potential and electric fields due to the effective density.
4. Interpolate the electric fields back to the particles using $W_i(r)$.

The PPPM method is closed related to the Ewald method. However, the cost of traditional Ewald summation scales as $N^{3/2}$ where N is the number of atoms in the system, while the PPPM solver scales as Nlog(N) due to the FFTs. According to the

study of Pollock[25], the Ewald method is suitable for systems of a few hundred particles per processor. For larger systems the PPPM algorithm is increasingly more efficient. Thus, for the system in this study, PPPM method is clearly the choice.

2.3. Boundary Conditions

Boundary conditions are crucial to simulations because it enables macroscopic properties to be calculated from simulations using relatively small number of atoms. For example, if we simulate 1000 water molecules in liquid state without a proper boundary condition, then most of the molecules would be influenced by the walls of the boundary. A simulation of this system would provide information about the liquid-solid interface not the bulk liquid properties. The surface effects can be removed by using periodic boundary conditions.

To implement periodic boundary condition in a simulation, imagine a volume V confining N atoms. The volume V is a primary cell which is replicated in all directions to give a periodic array. The replicas are called image cells. Each image cell contains N atoms which are images of the atoms in the primary cell. Each image atom has the same position and momentum and feels the same force as the corresponding atom in the primary cell. It can be proved that image atoms follow trajectories that are exact duplicated of those followed by the atoms in the primary cell. Any atom that leaves the primary cell is replaced by the image that simultaneously enters the primary cell. Thus, the use of periodic boundary conditions removes unwanted surface effects at the expense of introducing artificial periodicity in the system.

In this study, we employed periodic boundary conditions to ensure that the dicarboxylic acid coated nanoaerosol can evolve in an infinitely large vacuum environment.

2.4. Newtonian Dynamics

In molecular dynamics, the basic law that governs the motion of molecules is Newtonian dynamics. The Newton's law of motion can be summarized as follows:

1) In the absence of a net force, the center of mass of a body either is at rest or moves at a constant velocity.
2) A body experiencing a force **F** experiences an acceleration **a** related to **F** by **F** = *m***a**, where *m* is the mass of the body. Alternatively, force is equal to the time derivative of momentum.
3) Whenever a first body exerts a force **F** on a second body, the second body exerts a force −**F** on the first body. **F** and −**F** are equal in magnitude and opposite in direction.

In molecular dynamics simulation, the trajectory of a particle of mass m along one coordinate x with force F_x is obtained by solving the differential equations embodied in Newton's second law (F=ma):

$$\frac{d^2x}{dt^2} = \frac{F}{m}$$

2.5. Finite-Difference Method and Phase-Space Trajectories

In order to generate molecular trajectories, one needs to integrate the equation of motion. As we can see in section 2.2 about the intermolecular force field, the froce on

each atom will change as the atom changes its position or any of the other atoms it interacts changes position. Under the influence of this continuous force field, the motion of all atoms are coupled together, giving rise to a many-body problem that cannot be solved analytically. The classic tool for attacking this problem is finite-difference mehod.

2.5.1. Finiter Difference Method

In finite-difference method, differentials such as dx and dt are replaced by Δx and Δt, differential equations are replaced by finite-difference equations. The forces are assumed to be constant over a small time Δt. From the forces at time t, we can calculate the acceleration of an atom, combining the position and velocity at time t, we can calculate the position and acceleration at time t+ Δt.

The finte-difference method used in this study is the Verlet algorithm, which is one of the most widely used methods in molecular dynamics simulations. The Verlet algorithm uses the postions and accelerations at time t, and the positions from the previous step, to calculate the positions at t+ Δt. To derive this algorithm, we first write the Taylor series for position from time t forward to time t+ Δt:

$$\mathbf{r}(t+\Delta t) = \mathbf{r}(t) + \Delta t\mathbf{v}(t) + \tfrac{1}{2}t^2\mathbf{a}(t) + \mathrm{L}$$

then we write the Taylor series from t backward to t- Δt:

$$\mathbf{r}(t-\Delta t) = \mathbf{r}(t) - \Delta t\mathbf{v}(t) + \tfrac{1}{2}\Delta t^2\mathbf{a}(t) - \mathrm{L}$$

Adding these two equation gives:

$$\mathbf{r}(t+\Delta t) = 2\mathbf{r}(t) - \mathbf{r}(t-\Delta t) + \Delta t^2\mathbf{a}(t)$$

This is Verlet's algorithm for positions. It has a local truncation error that varies as $(\Delta t)^4$ and hence is a third order method. We can see that the velocities do not explicitly appear in the Verlet algorithm. To calculate the velocities, one way is to use central difference estimator:

$$\mathbf{v}(t) \approx \frac{\mathbf{r}(t+\Delta t) - \mathbf{r}(t-\Delta t)}{2\Delta t}$$

Alternatively, the velocities can be estimate at the half-step as:

$$\mathbf{v}(t+\tfrac{1}{2}\Delta t) \approx \frac{\mathbf{r}(t+\Delta t) - \mathbf{r}(t)}{\Delta t}$$

The Verlet algorithm offers the virtues of simplicity and good stability for moderatedly large time steps. One drawback of this algorithm is that the positions at t+ Δt are obtained by adding a small term $\Delta t^2 \mathbf{a}(t)$ to the difference of two larger terms $2\mathbf{r}(t)$ and $\mathbf{r}(t-\Delta t)$. This may result in loss of precision[18]. Another drawback is that the Verlet algorithm is not self-starting, since initial positions and velocities are not sufficient to begin a simulation and another method must be used to get $\mathbf{r}(-\Delta t)$.

Several variations on the Verlet algorithm have been deceloped to overcome the drawbacks of the orginal Verlet algorithm. One of the variations is velocity Verlet algorithm. It gives positions, velocities and accelerations at the same time and does not compromise precision:

$$\mathbf{r}(t+\Delta t) = \mathbf{r}(t) + \Delta t \mathbf{v}(t) + \tfrac{1}{2} t^2 \mathbf{a}(t)$$

$$\mathbf{v}(t+\Delta t) = \mathbf{v}(t) + \tfrac{1}{2}\Delta t[\mathbf{a}(t) + \mathbf{a}(t+\Delta t)]$$

The advantages of this algorithm are self-starting, time reversible and symplectic (preserves volume in phase space).

2.5.2. Phase-Space Trajectories

In computer simulation, the idea of trajectory includes not only positions but also moleular momenta. For an isolated system, the particles move according to Newton's law of motion and generate trajectories which can be represented by time-dependent position vectors. As the particles follow their trajectories, the forces on the particles also change with time, which leads to time-dependent momentum vectors.

For a system consists of N particles, at one instant, 6N values are needed to define the state of the system, 3N for positions and 3N for momentum. Imaging plotting the positions and momenta of the N particles at any instant in a hyperspace, then 6N dimensions are needed. Such a space is called phase space, in which 3N dimensions are for configuration and 3N dimensions are for momentum. At one instant, the positions and momenta of the system are represented by one point in this space. As the system envolves with time, the point moves, describing a trajectory in phase space. An ensemble can be considered to be a collection of points in phase space. These points correspond to the successive configureations of the system generated by the simulation. An NVE molecular dynamics simulation (microcanonical ensembel) samples the points in phase space along a constant energy line.

2.5.3. Ergodicity

An important concept in phase space is ergodicity[18]. A system is ergodic if over a sufficiently long time the phase space point passes through all configurations on the constant-Hamiltonian surface. A closely related concept is quasi-ergodicity which means over a sufficiently long time the phase space point passes arbitrarily close to

all configurations. However, under these definitions of ergodicity, real dynamical systems in three dimension are neither ergodic nor quasi-ergodic.

For a system to evolve from nonequilibrium states to equilibrium states, two conditions must be satisfied[18]. First, the full constant-Hamiltonian surface must be accessible. Second, the phase space trajectory must be unstable to small perturbations, i.e. a perturbed trajectory must drift away from its unperturbed parent trajectory, and the degree of instability must be at least mixing, which is the lowest level of unstable motion.

2.6. Static and Dynamic Properties

By analyzing phase space trajectories, we can evaluate macroscopic properties which can be divided into two kinds: static properties and dynamic properties. Static properties include thermodynamic properties and static structure properties. Dynamic properties include time correlation functions, thermal transport coefficients and dynamic structure properties[19].

2.6.1. Time Averages and Ensemble Averages

To determine the macroscopic properties of a system, one needs to distinguish between time averages and ensemble averages. Consider N particles that comprise the system. The instantaneous value of the property A can be written as $A(\mathbf{p}^N(t), \mathbf{r}^N(t))$, where $\mathbf{p}^N(t)$ and $\mathbf{r}^N(t)$ represent the N momenta and positions at time t. The value of A fluctuates over time as a result of interactions between particles. As the time over which the measurement is made goes to infinity, the time average represented by the following integral approaches the 'true' average value of the property:

$$A_{ave} = \lim_{\tau \to \infty} \frac{1}{\tau} \int_{t=0}^{\tau} A(\mathbf{p}^N(t), \mathbf{r}^N(t)) dt$$

In statistical mechanics, a single system evolving in time is replaced by a large number of replications of the system that are considered simultaneously. The time average is replaced by an ensembel average which is an average taken over a large number of replicas of the system:

$$\langle A \rangle = \iint A(\mathbf{p}^N, \mathbf{r}^N) \rho(\mathbf{p}^N, \mathbf{r}^N) d\mathbf{p}^N d\mathbf{r}^N$$

Here, the angle brackets $\langle\ \rangle$ indicate an ensemble average. $\rho(\mathbf{p}^N, \mathbf{r}^N)$ is the probability density of the ensemble, i.e. the probability of finding a configuration with momenta $\mathbf{p}^N(t)$ and positions $\mathbf{r}^N(t)$ .Thus, the ensemble average of the property A is the expectation value over all possible configurations of the system. In statistical mechanics, the average corresponding to experimental observables are defined in terms of ensemble averages. Under conditions of constant number of particles, volume and energy (constant NVE), the probability density function is the well-known Boltzmann distribution:

$$\rho(\mathbf{p}^N, \mathbf{r}^N) = e^{\frac{-E(\mathbf{p}^N, \mathbf{r}^N)}{k_B T}} / Z$$

In this equation, $E(\mathbf{p}^N, \mathbf{r}^N)$ is the energy, Z is the partition function, k_B is the Boltzmann's constant and T is the temperature. The partition function is given by:

$$Z = \iint e^{\frac{-E(\mathbf{p}^N, \mathbf{r}^N)}{k_B T}} d\mathbf{p}^N d\mathbf{r}^N$$

To calculate the ensemble average in a molecular dynamics simulation, the MD simulation must pass through all the possible states corresponding to the particular thermodynamic constraints. However, what is actually done in a molecular dynamics

simulation, is to detemine an average value of A over a time interval t starting from time t_0:

$$A_m = \frac{1}{t}\int_{t_0}^{t_0+t} A(\mathbf{p}^N(\tau), \mathbf{r}^N(\tau))d\tau$$

For a system at equilibrium, the above average is independent of starting time. Moreover, we assume that this average reliably approximates the time average A_{ave}. Then, the dilemma appears to be that one calculates time averages by MD simulations, but the experimental observables are assumed to be ensemble averages. Resolving this leads to one of the most fundamental axioms of statistical mechanics, the ergodic hypothesis, which states that the time average equals the ensemble average:

$$A_{ave} = \langle A \rangle$$

In other words all parts of the phase space are sampled.

2.6.2. Static Properties

The static properties calculated in this study are reviewed in this section. Those properties include internal energy, temperature and radial distribution function.

Internal Energy: For an isolated system, the total internal energy is a constant, which divides into a kinetic part E_k and a configurational part U. The average kinetic energy is proportional to the absolute temperature.

$$\langle E_k \rangle = \frac{1}{2mM}\sum_{k=1}^{M}\sum_{i=1}^{N}\mathbf{p}_i(k\Delta t)\cdot\mathbf{p}_i(k\Delta t)$$

where m is the mass of one particle. The configurational internal energy is the average of the pair potential function u(r).

$$\langle U \rangle = \frac{1}{M} \sum_{k=1}^{M} \sum_{\boldsymbol{\alpha}} \sum_{i<j} \sum u\left[\left| \mathbf{r}_{ij}(k\Delta t) - \boldsymbol{\alpha} L \right| \right]$$

where $r_{ij} = \left| \mathbf{r}_i - \mathbf{r}_j \right|$ is the distance between the centers of atom i and j. L is the length of one side of the primary cell, and $\boldsymbol{\alpha}$ is the cell translation vector in periodic boundary condition.

Temperature: In the microcanonical ensemble, the temperature will flutuate. The temperature is directly related to the kinetic energy of the system as follows:

$$\langle E_k \rangle = \frac{k_B T}{2}(3N - N_c)$$

where N_c is the number of constraints on the system. According to the equipartition theorem, if there are N particles, each with three degrees of freedom, the the kinetic energy should equal $3Nk_BT/2$. In MD simulation, the total linear momentum of the system is often constrained to zero, which means three degrees of freedom are removed from the system.

Radial Distribution Function: The radial distibution function g(r) measures the "local structure" of the system i.e. how atoms organize themselves around one another. It is a measure of, on average, the probability of finding a particle at a distance of *r* away from a given reference particle, relative to that for an ideal gas. The radial distribution function is a useful tool to describe the microstructure of a system, particularly of liquids. In a crystal, the radial distribution function has an

ifinite number of sharp peaks whose separations and heights are characteristic of the lattice structure. Liquids exhibit short-range order similar to that in crystals, but long-range disorder like that in gases. Thus, the radial distribution function of liquids or amorphous solids is intermediate between the solid and the gas, with a small number of peaks as short distances, superimposed on a steady decay to a constant value at longer distances. A typical radial distribution function calculated from a MD simulation is shown in Figure 2.4.[19] As we can see from the figure, at short distances (less than atomic diameter) g(r) is zero. This is due to the strong repulsive forces. The first (and large) peak occurs at $r \approx 3.7$ Å, with g(r) having a value of about 3. This means that it is three times more likely that two molecules would be found at this separation. The radial distribution function then falls and passes through a minimum value around $r \approx 5.4$ Å. The chances of finding two atoms with this separation are less. At long distances, g(r) approaches one which indicates there is no long-rang order. The radial distribution function depends on density and temperature, therefore, in computer simulation studies, g(r) serves as a helpful indicator of the nature of the phase. This function can also be used to compute the ensemble average of any pair function. To calculate the pair distribution function from a simulation, the neighbors around each atom or molecule are sorted into distance bins. The number of neighbors in each bin is averaged over the entire simulation.

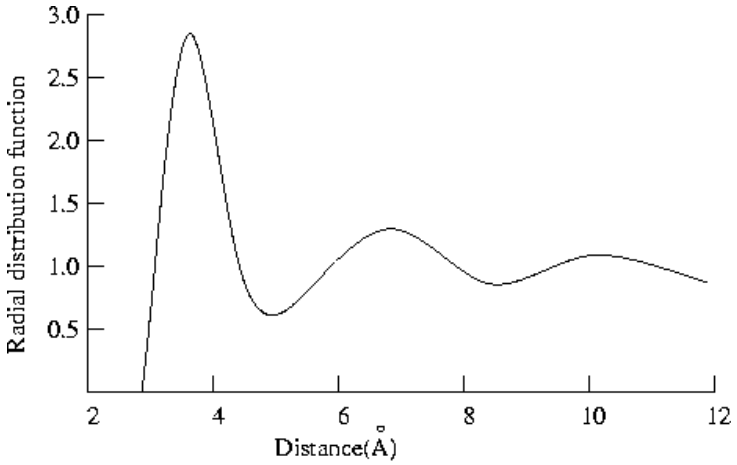

Figure 2.4. Radial distribution function of liquid argon

Radial Density Function: The density of the system was calculated as a function of radial distance. To calculate density, we considered a shell of thickness δr at a distance r from the center of mass. The density at radial distance r is given by the mass of all the sites in that shell divided by the volume of the shell.

2.6.3. Dynamic Properties

Dynamic (time-dependent) properties of the system include time correlation functions, thermal transport coefficients, and dynamic structure. The capability to calcualte system dynamic properties is a major advantage of molecular dynamics simulation over the Monte Carl method. In this study, we calculated the diffusion coefficients of water and dicarboxylic acid molecule in different nanoaerosol environments. The diffusion coefficient is related to the mean square distance, $\left\langle \left| [\mathbf{r}(t) - \mathbf{r}(0)]^2 \right| \right\rangle$ according to the Einstein equation. In three dimensions, the equation is given below: $\lim_{t\to\infty} \frac{\left\langle \left| [\mathbf{r}(t) - \mathbf{r}(0)]^2 \right| \right\rangle}{2t} = 3D$ This relationship strictly holds only in the

limit as $t \to \infty$ .The Einstein relationship can be used to calculate the diffusion coefficient from an equilibrium simulation by plotting the mean square displacement as a function of time and then attempting to obtain the limiting behavior as $t \to \infty$. The calculation can be averaged over the particles in the system to reduce the statistical error.

Chapter 3: LAMMPS Software and Simulation Details

3.1. LAMMPS Software

The simulations in this work were carried out using the open source software package LAMMPS[26] (Large-scale Atomic/Molecular Massively Parallel Simulator, http://lammps.sandia.gov/). It is a classical molecular dynamics simulation code developed by Steve Plimpton at Sandia National Laboratories and designed to run efficiently on parallel computers. The general features of the LAMMPS include:

- runs on a single processor or in parallel
- distributed-memory message-passing parallelism (MPI)
- spatial-decomposition of simulation domain for parallelism
- open-source distribution
- highly portable C++
- optional libraries used: MPI and single-processor FFT
- easy to extend with new features and functionality
- runs from an input script
- syntax for defining and using variables and formulas
- syntax for looping over runs and breaking out of loops
- run one or multiple simulations simultaneously (in parallel) from one script

3.2. Parallel Algorithms

Three classes of parallel algorithms for classical molecular dynamics have been proposed[26]. In the first class of methods, a pre-determined set of force computations

is assigned to each processor. The assignment remains fixed for the duration of the simulation. This method is called an atom-decomposition of the workload. Atoms in a group need not have any special spatial relationship. The drawback of this method is that every time step each processor must receive updated atom positions from all the other processors, an operation called all-to-all communication. This communication scales as N, independent of P, so it limits the number of processors that can be used effectively. The second class of methods assigns each processor a fixed subset of inter-atomic forces. It is called a force-decomposition of the workload. This block-decomposition of the force matrix only needs $O(N/\sqrt{P})$ information to perform its computations. Thus the communication cost scales as $O(N/\sqrt{P})$. The third class of parallel algorithms divides the physical simulation domain into small 3D boxes, one for each processor. It is called a spatial-decomposition of the workload and it is used in the LAMMPS software. Each processor computes forces on and updates the positions and velocities of all atoms within its box at each time step. The size and shape of the box assigned to each processor depends on N, P and the aspect ratio of the physical domain. The number of processors in each dimension is chosen so as to make each processor's box as cubic as possible. The details of the communication scheme used to acquire information from processors can be found in reference [26]. Like the atom-decomposition and force-decomposition algorithms, the spatial-decomposition method evenly divides the MD computations across all the processors. Its chief benefit is that it takes full advantage of the local nature of the inter-atomic forces by performing only local communication. Thus, for large scale MD simulation, it can achieve optimal $O(N/P)$ scaling and is clearly the fastest algorithm. Like other

parallel algorithms, spatial-decomposition also has some drawbacks. First, since the performance of this method is sensitive to the problem geometry, it is more restrictive than the other algorithms. Second, due to the complexity of this algorithm, it is more difficult to implement efficiently than other algorithms. It also requires extra coding and a substantial reworking of data structures.

3.3. Simulation Details

3.3.1. Simulating the Water Core

The first step toward building a dicarboxylic acid coated aqueous aerosol was to build a pure water droplet. The detailed procedures for preparing an equilibrated water droplet are described in our previous work[7]. In brief, the water droplet is evolved from a simple cubic lattice structure with the oxygen atom at the vertex of each cube. The initial sphere configuration consisting of 2440 water molecules was generated by considering only the water molecules inside a sphere of a certain radius. The water droplet is equilibrated at the temperature of 260K. The SHAKE algorithm[23] was used to apply constraints between O-H bond and H-O-H angle to maintain the rigidity of the water molecules. The radial distribution function confirms the liquid phase of the prepared water droplet.

3.3.2. Simulating the Dicarboxylic Acid Molecule

The next step was to coat the spherical water droplet with dicarboxylic acid molecules. By identifying the surface molecules of the water droplet, we placed dicarboxylic acid molecules on each surface water site with one of the carboxyl group

of the dicarboxylic acid attached to the surface water molecule and the straight hydrocarbon chain of the dicarboxylic acid placed radially outward.

The dicarboxylic acids simulated were malonic acid (C3), succinic acid (C4), glutaric acid (C5), adipic acid (C6), pimelic acid (C7), suberic acid (C8), azelaic acid (C9) and branched azelaic acid (C9b). The details of the force fields used to model the dicarboxylic acid molecules were discussed in section 2.2.2.

3.3.3. Equilibration Procedures

After attaching a monolayer dicarboxylic acid to the surface of water droplet, an energy minimization run was performed using the conjugate gradient (CG) algorithm to relax the initial configuration containing highly overlapped atoms. The system was then allowed to equilibrate at 0K for 10ps using constant NVE integration with velocity-Verlet algorithm to update position and velocity for atoms. A timestep of 1fs was typically chosen to ensure the energy conservation. During the equilibration process, the temperature was controlled by rescaling the velocities every timestep. After the system relaxation at 0K, the coated particle was slowly heated to 260K within 20ps and then allowed to equilibrate for 40ps. Following that, the system was heated to 300K and allowed to equilibrate at that temperature for up to 8ns. For the final step of the preparation process, the simulations were switched from a constant temperature to a constant energy calculation to ensure that the average system temperature did not deviate by more than 10K. The simulations were carried out in a constant energy environment during the data generation phase. All the simulations were run on a Linux cluster, running in parallel on 8 processors.

3.4. Some Practical Issues

3.4.1. Choosing the Initial Configuration

It is necessary and important to select an initial configuration of the system before a simulation can be perform since the initial arrangement can often determine the success or failure of a simulation. There are no hard rules for choosing the most appropriate initial configurations in molecular dynamics simulations. However, there exist some general rules which can help us select the right one. The initial configuration can be obtained from experimental data, from a theoretical model or from a combination of both. For simulations of systems at equilibrium, it is wise to choose an initial configuration that is close to the state which it is desired to simulate. It is also important to ensure that the initial configuration does not contain any high energy interactions such as overlaps as these may cause instabilities in the simulation. Performing energy minimization prior to the simulation is a good way to eradicate these high energy 'hot spots'.

In our simulation, we start with an initial 'inverted micelle' configuration. This model consisting of an aqueous core that is encapsulated in an inert, hydrophobic organic monolayer is stimulated by field measurements. The organic materials that coat the aerosol particles are surfactants of biological origin. In this model, the surfactants lie with their polar heads inserted into the ionic aqueous core with their hydrophobic hydrocarbon tails exposed to the atmosphere. Wyslouzil et al.[27] have shown, using small angle neutron scattering, evidence for surface segregation of organic/water systems.

3.4.2. Choosing an Appropriate Time Step

As in choosing the initial configuration, there are no hard and fast rules for calculating the most appropriate time step to use in a molecular dynamics simulation. Too small and the trajectory will cover only a limited proportion of the phase space; too large the instabilities may arise in the integration algorithm due to high energy overlaps between atoms. Such instabilities would certainly lead to a violation of energy and linear momentum conservation and could result in a program failure due to numerical overflow. A general requirement is that the time step is approximately one order of magnitude smaller that the shortest motion[19]. The following table lists some suggested time steps in MD simulations. In our simulation, we used a time step of 1fs during the equilibration process.

System	Types of motion present	Suggested time step (fs)
Atoms	Translation	10
Rigid molecules	Translation and rotation	5
Flexible molecules, rigid bonds	Translation, rotation, torsion	2
Flexible molecules, flexible bonds	Translation, rotation, torsion, vibration	1 or 5

Table 3.1. Different types of motion present in various systems together with suggested time steps.

3.4.3. Monitoring Equilibrium

From thermodynamics, a necessary and sufficient condition for identifying equilibrium is that the system entropy be a maximum. However, entropy is not a

measurable property and cannot be evaluated from the time average of some mechanical quantity. Equilibrium is a macroscopic concept. It applies over a finite duration to a system of macroscopic size. Equilibrium pertains to a finite duration that is important to the observer[18]. Some necessary conditions for an isolated system at equilibrium are as follows:

1. The total number of atoms N and total energy E should be constants, independent of time. Thus, fluctuations in the kinetic energy and potential energy must be equal in magnitude but out of phase with each other.

2 Each Cartesian component of the velocities should, on a time average, describe a Maxwell distribution.

3. Thermodynamic properties, such as the temperature, pressure should be fluctuating about average values.

4. Property averages should be stable to small perturbations.

5. If the system is divided into parts, time average for each property should be the same in each part.

3.4.4. Constraint Dynamics: SHAKE Algorithm

When simulating flexible molecules, the conformational behavior of the molecule is usually a complex superposition of different motions. The high frequency motions (e.g. bond vibrations) are usually of less interest than the lower frequency motions. Unfortunately, the time step of a molecular dynamics simulation is dictated by the highest frequency motion in the system. In order to increase the time step without prejudicing the accuracy of the simulation, individual internal coordinates have to be constrained or ‘fixed’ during the simulation without affecting the other internal

degrees of freedom. The most commonly used method for applying constraints in molecular dynamics is the SHAKE algorithm developed by Ryckaert et al[23]. SHAKE algorithm deals with holonomic constraints which can be expressed in the form:

$$f(q_1, q_2, q_3, ...t) = 0$$

The SHAKE method solves the constraints using Lagrange multipliers. When there are many constraints, each constraint is considered in turn and solved. Satisfying one constraint may cause another constraint to be violated, and so it is necessary to iterate around the constraints until they are all satisfied to within some tolerance. Angle constraints can be easily accommodated in the SHAKE algorithm by recognizing that an angle constraint corresponds to an additional distance constraint. For example, the angle in a tri-atomic molecule could be maintained at the desired value by requiring the distance between the two end atoms to adopt the appropriate value. An example for this would be the simple water models in which the HOH angle is fixed. The most common use of SHAKE is for constraining bonds involving hydrogen atoms due to their much higher vibrational frequencies. In our simulation, the SHAKE algorithm was used to apply constraints between O-H bond and H-O-H angle to maintain the rigidity of the water molecules.

Chapter 4: Structures of Dicarboxylic Acid Coated Aqueous Nanoaerosol

In this section, the results from the molecular dynamics simulations are presented and discussed. In order to study the effect of dicarboxylic acid chain length on the structure of coated nanoaerosols, we computed many physical properties of the systems, including radial density distributions, radial distribution functions and diffusion coefficients.

4.1. Structure

The time evolutions of different dicarboxylic acids coated nanoaerosol structures were monitored during the simulation process. Different equilibrium morphologies were observed. Figure 4.1.(a) shows the cross-sectional view of the C3-coated nanoaerosol at various stages of the simulation. As we can see from the images, the C3 molecules slowly migrated from the surface to the core of the nanoaerosol and mixed with the water molecules during the simulation. After about 1ns of equilibration, all the surface C3 molecules dissolved into the water droplet and mixed with the surface water molecules. After about 5-6ns, the C3 molecules dissolved further into the water core and distributed around the center of the nanoaerosol. The whole nanoaerosol looks like a “bigger” water droplet from the outside.

The evolution paths of C5-C9 coated nanoaerosols are similar but are different from that of C3 coated nanoaerosol. As a representative, the initial and final morphologies of C8 coated nanoaerosol are presented in Figure 4.1.(b) for comparison. As we can see from the images, phase separation was observed at the

surface of the water droplet. Initially, the C8 molecules were uniformly distributed on the surface of the water droplet with the straight chain of the dicarboxylic acid placed radially outward. During the simulation, the acid molecules tended to clump together and formed a layered droplet while the water cluster was “squeezed” to the other side of the nanoaerosol. This observed phase separation is similar to that of mixing oil and water. Since an acid molecule does not hydrogen bond with a water molecule, an acid’s dispersion attraction to a water molecule is weaker than the acid-acid attraction. Therefore, the water cluster stays separate from the dicarboxylic acid molecules during the equilibration process. Due to the low water solubility of long chain dicarboxylic acids, phase separation was also observed among C5-C9 coated nanoaerosols. The equilibrated structure of C4 coated nanoaerosol is the transition between the other two cases with some of the acid molecules dissolved into the water core and the other acid molecules formed a separate acid cluster.

To investigate the effect of branched chain on the structure evolution of dicarboxylic acid coated nanoaerosol, C9 molecule was modified to add two side CH_2 groups forming C9-branched molecule. Figure 4.1.(c) shows the initial and final structures of this system. Different from previous cases, the C9_branched acid molecules did not dissolve into the water droplet or form a separate acid cluster on the water droplet surface. The acid molecules only slightly bended and the water core remained almost intact. The addition of two side CH_2 groups thus immobilized the motion of acid molecules and stabilized the structure of the nanoaerosol.

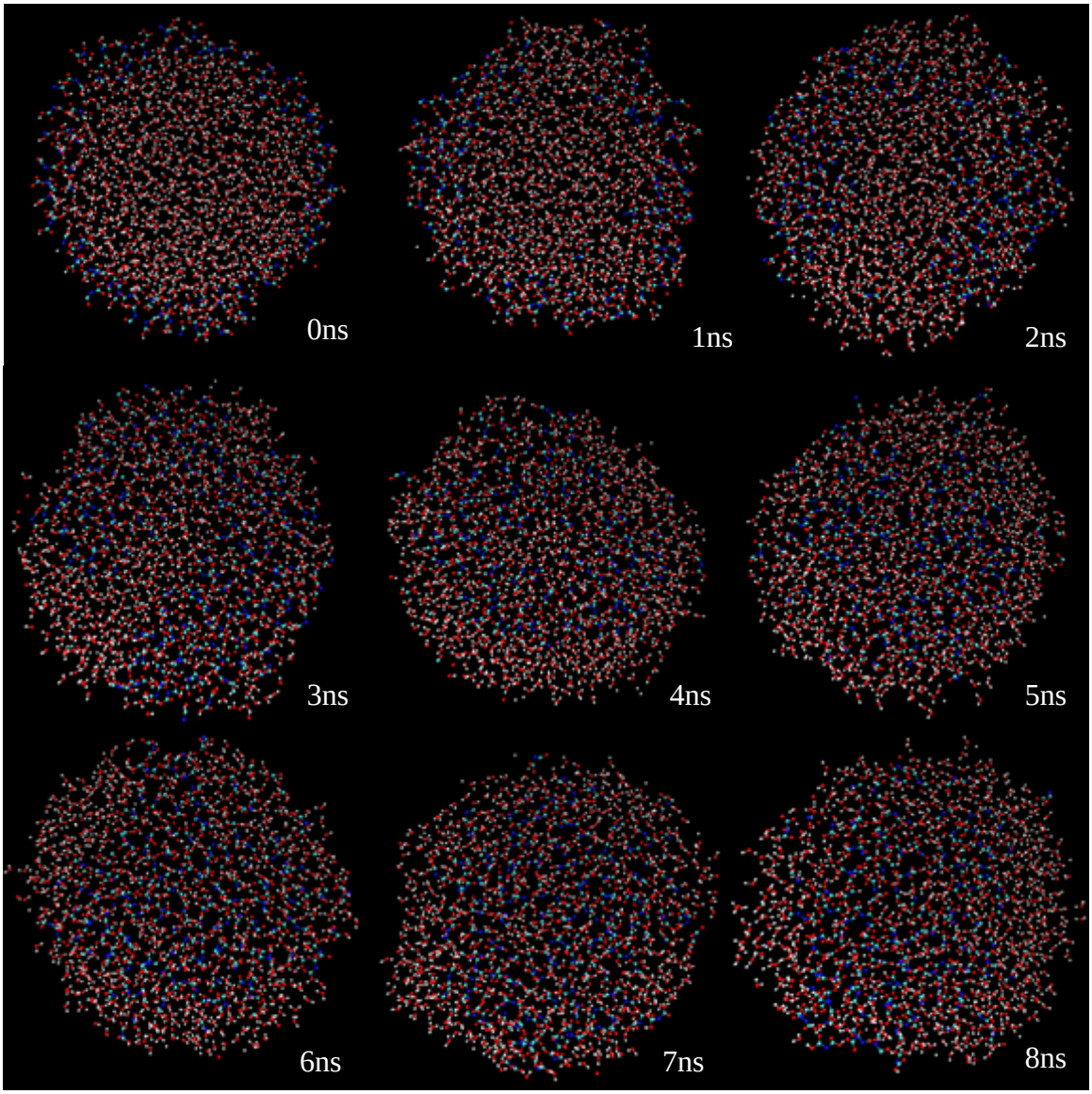

(a)

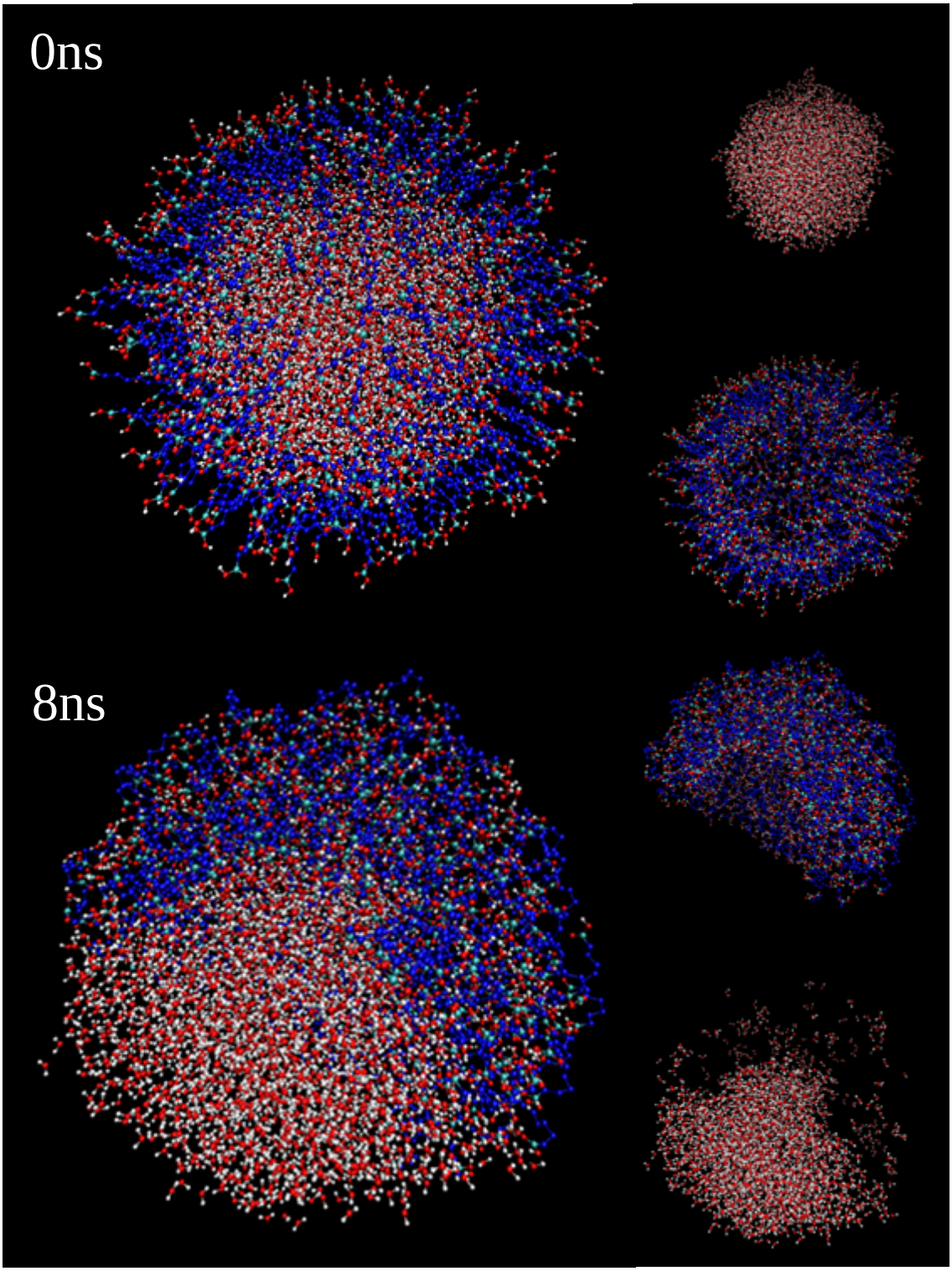

(b)

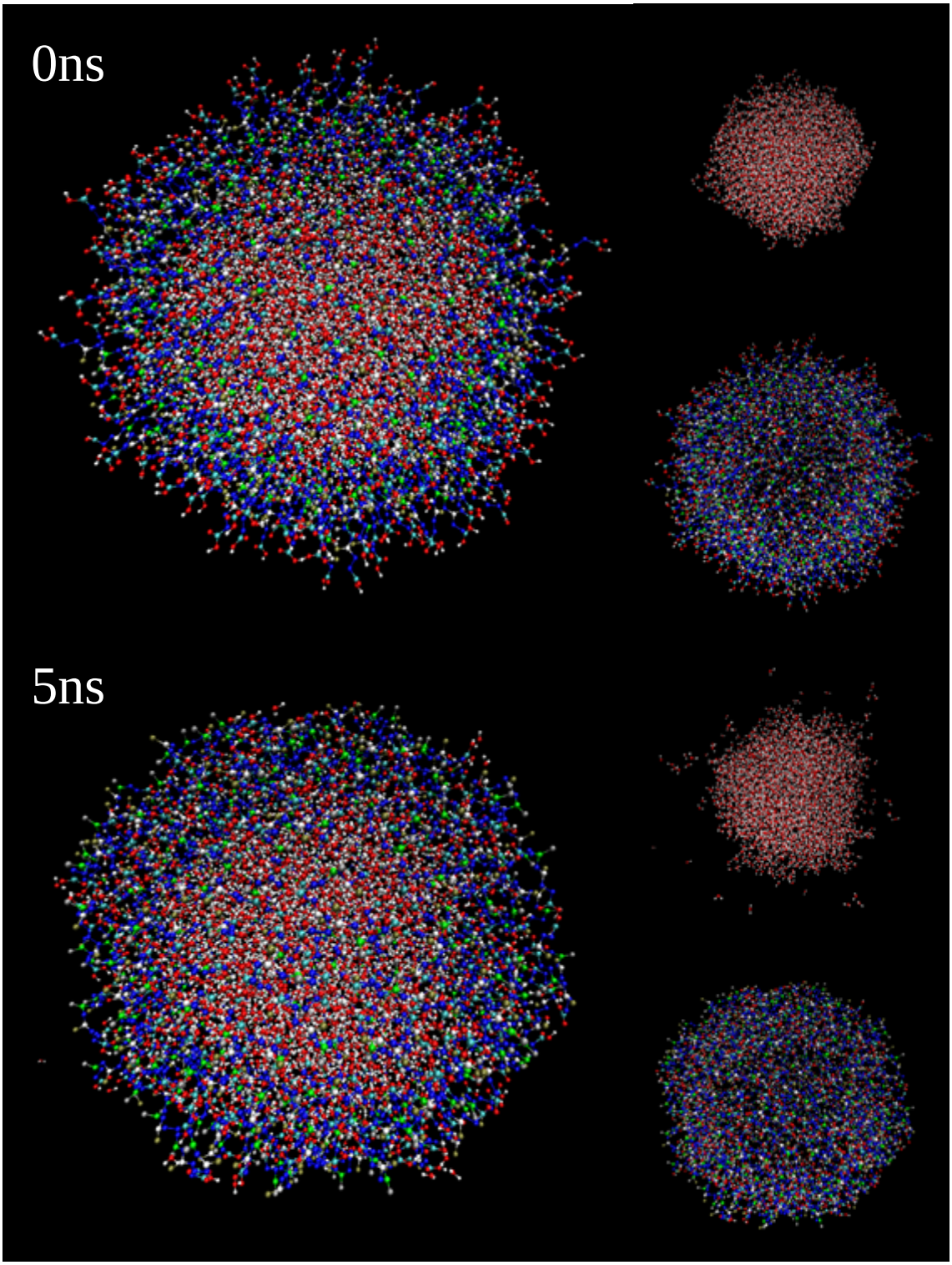

(c)

Figure 4.1.(a). Structures of dicarboxylic acid coated nanoaerosols (a) cross-sectional view of C3 coated nanoaersol at different

stages of equilibration (b) structure of C8 coated nanoaerosol (c) structure of C9_branched coated nanoaerosol

4.2. Radial Density

The density profiles of the dicarboxylic acid coated nanoaerosols were calculated as a function of radial distance r. To calculate density, we considered a shell of thickness δr at a distance r from the center of mass. The density at radial distance r is given by the mass of all the sites in that shell divided by the volume of the shell. Due to the lack of spherical symmetry, the density calculation could not be performed on C4-C9 dicarboxylic acid coated nanoaerosols. The calculated density profiles for C3 and C9_branched dicarboxylic acid coated nanoaerosols are presented in Figure 4.2.

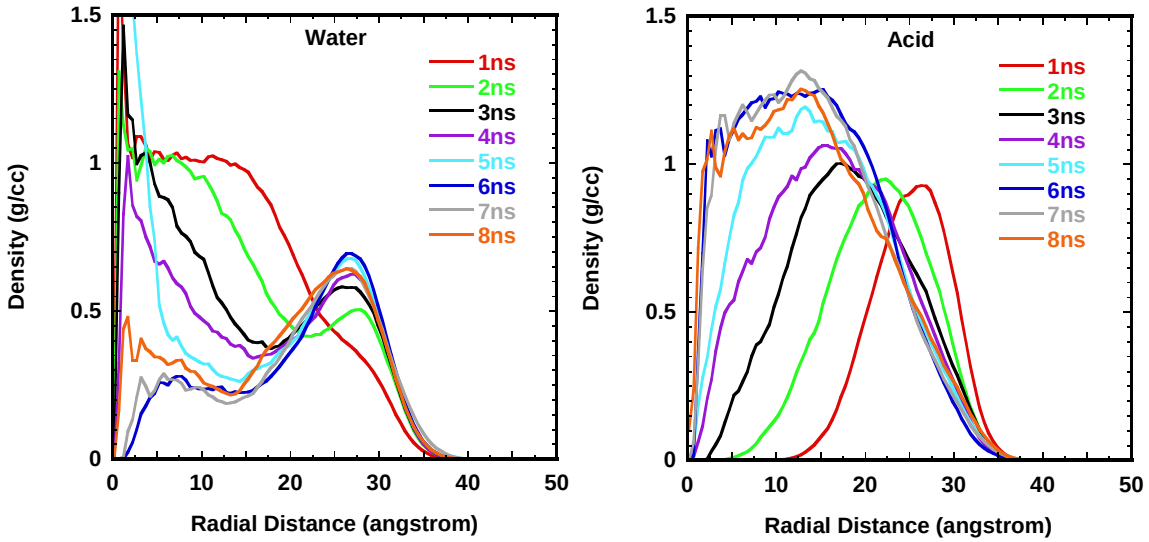

(a)

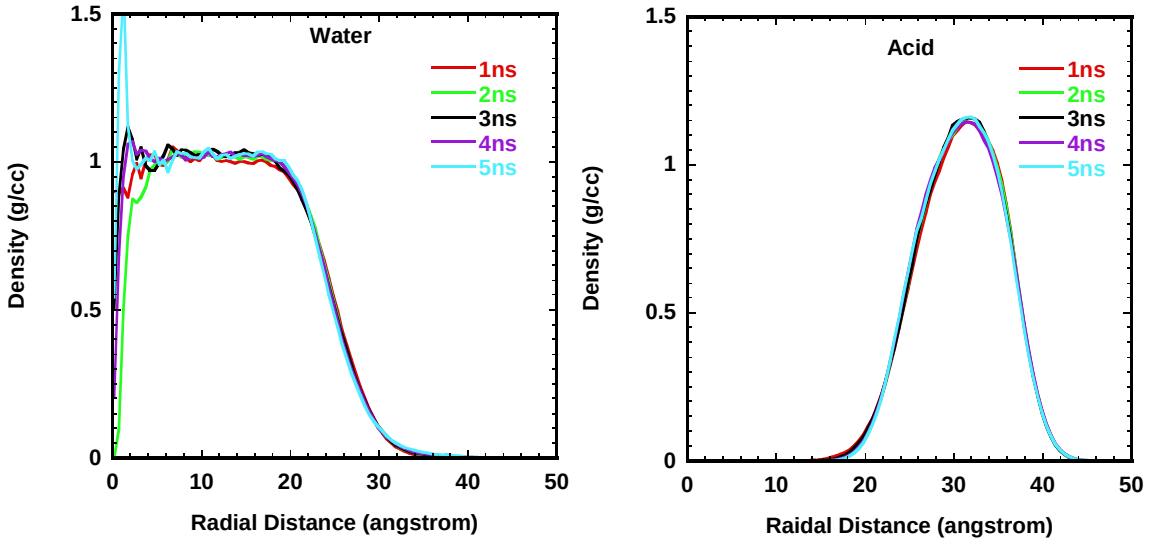

(b)

Figure 4.2. Radial density distributions of C3 and C9_branched acids coated nanoaerosols as a function of simulation time

As we can see from the figure 4.2.(a), for C3 acid coated nanoaerosol, the acid density distribution gradually shifted to the inside of the aerosol which indicates dissolution of the acid molecules into the water. At the same time the water density profiles show that water is essentially being squeezed out of the core by the acid molecules, and a very low water density is observed at the central region of the aerosol. After about 5-6ns of equilibration, both water and acid density profiles became stable which means equilibrium structures was achieved. Compared with the C3 coated nanoaerosol, the density profiles of C9_branched acid coated nanoaerosol did not vary much during the whole equilibration process. The calculated density profiles are consistent with the structure evolutions of the nanoaerosols.

4.3. Radial Distribution Function

The radial distribution function (RDF), g(r), is defined as the number of atoms a distance *r* from a given atom compared with the number of atoms at the same distance in an ideal gas. It is a useful tool to describe the structure of a system, particularly of liquids. To calculate the radial distribution function, the neighbors around each atom or molecule are sorted into distance bins. The number of neighbors in each bin is then averaged over the simulation.

In our simulation, the radial distribution function for each atom pair is histogrammed into 100 bins from distance 0 to the maximum force cutoff distance. To investigate the microstructure changes of the dicarboxylic acid coated nanoaerosols, radial distribution functions between different atom pairs were calculated. The RDF of water oxygen-oxygen pair was calculated to characterize the changes in water structure. The RDF of atom pair between the water oxygen and the carbon atom in the acid head group was calculated to monitor the relative structure changes between water and acid. The RDF of acid central CH_2-CH_2 groups was calculated to characterize the structure changes between dicarboxylic acid molecules. The RDF results for representing nanoaerosols are presented in Figure 4.3.

Figure 4.3.(a) shows the water oxygen-oxygen RDFs for C3, C8 and C9_branched acid coated nanoaerosols after the equilibration process. For all three RDFs, the major peak occurs at roughly 2.8Å which is the well-known average hydrogen bond length in water. The lack of peaks at long distances indicates there is no long-rang order for water. Figure 4.3.(b) compares the RDFs of acid central CH_2-CH_2 groups for the three representing nanoaerosols after the equilibration. It can be seen that the RDF for C3

coated nanoaerosol clearly exhibits a peak at around 5Å, while the RDFs for C8 and C9_branched coated nanoaerosol only have a smaller and broader peak at longer disances. The reader is reminded that in the final equlibrium stage, the coating C3 acid molecules all dissolved into the water core. Thus, a clear peak in the RDF indicates that C3 acid molecules formed a short-range ordered structure in water. The time evolution of the RDFs of acid central CH_2-CH_2 groups in C3 coated nanoaerosol is presented in Figure 4.3.(c). As the system evolves with time, the peaks in RDFs grow which indicates the gradual formation of an ordered structure. A snapshot of C3 acid molecules in the equlibrium phase is shown in Figure 4.4. (For emphasizing, water molecules are removed). As we can see from the figure, C3 acid molecules tend to stay in parallal with each other and form a spherical cluster with layered structure. This ordered structure lows the energy of the system. To investigate the phase separation process occuring in long chain dicarboxylic acids coated nanoaerosols, the RDFs of atom pair between the water oxygen and the carbon atom in the acid head group were calculated at different stage of equilibration. The results for C8 coated nanoaerosol are presented in Figure 4.3.(c). As we can see from the figure, starting from the initial “ordered configuration” where all the acid molecules pointing radially out of the water droplet, the peaks in the RDFs continuously shrunk in size accompanied by the decrease in intensity at different distances. The decrease in RDF intensity indicates the enlargement in the separation between water molecules and acid molecules.

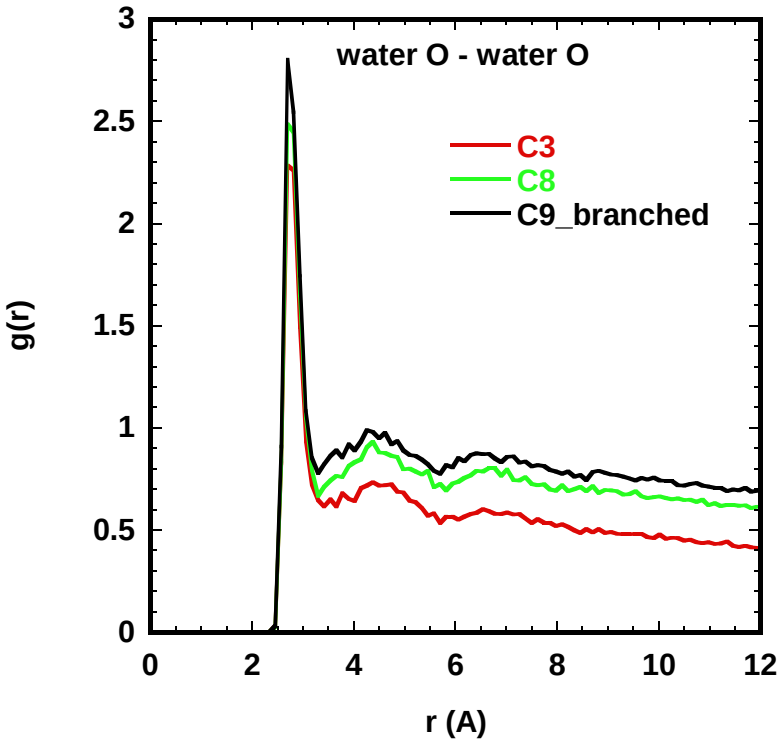
water O - water O
C3
C8
C9_branched
g(r)
r (A)
0
0.5
1
1.5
2
2.5
3
0
2
4
6
8
10
12

(a)

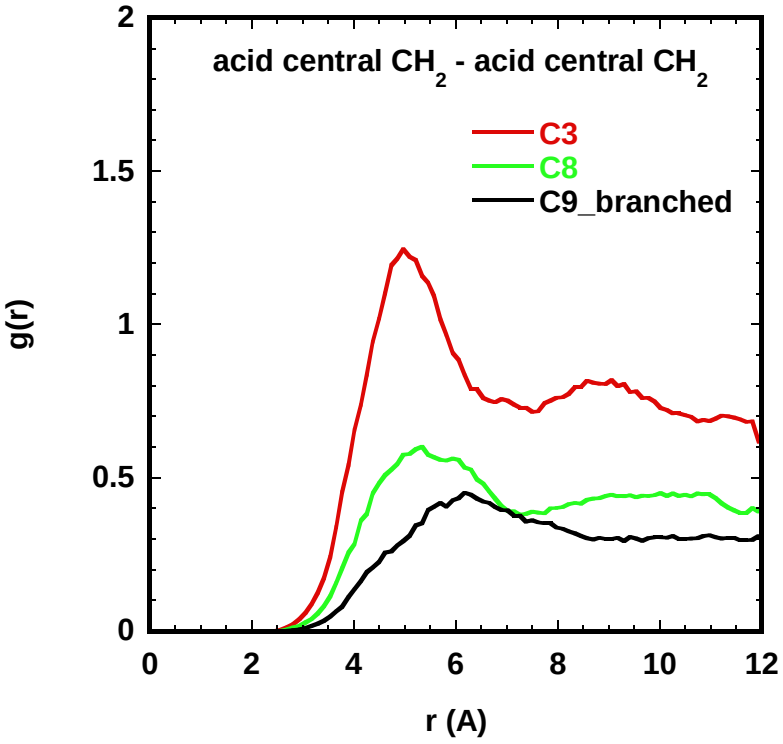
acid central CH2 - acid central CH2
C3
C8
C9_branched
g(r)
r (A)
0
0.5
1
1.5
2
0
2
4
6
8
10
12

(b)

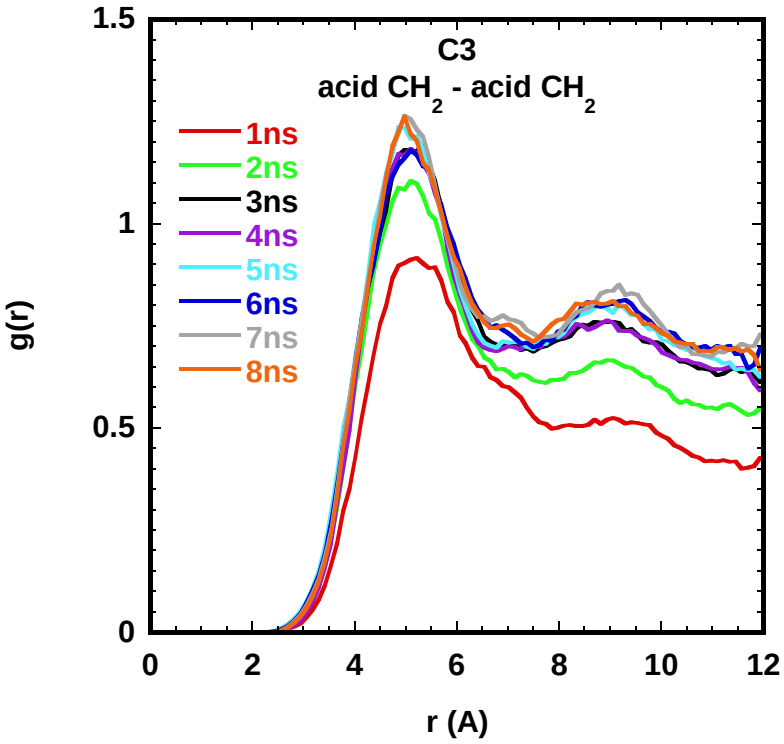
C3
acid CH2 - acid CH2
1ns
2ns
3ns
4ns
5ns
6ns
7ns
8ns
g(r)
r (A)
0
0.5
1
1.5
0
2
4
6
8
10
12

(c)

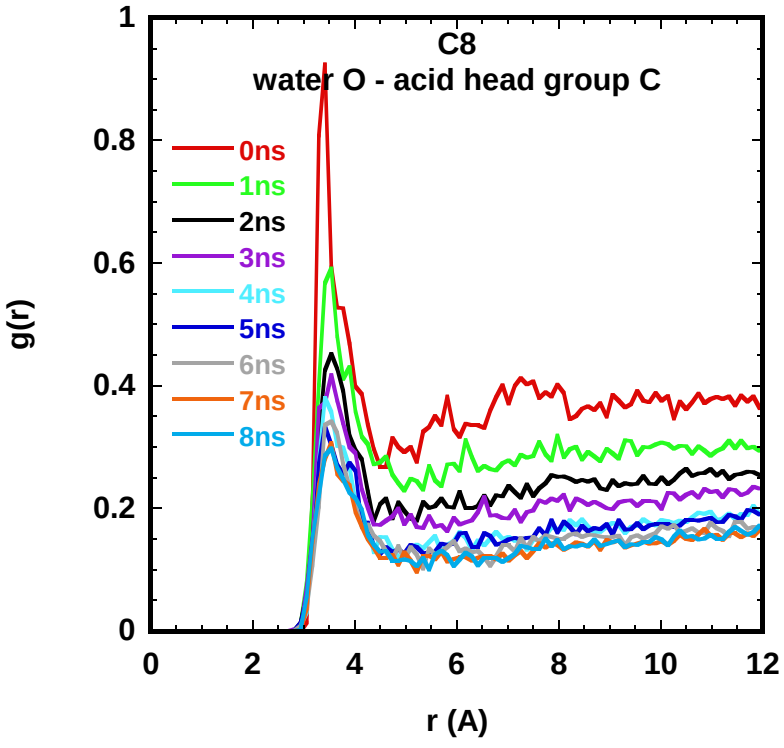
C8
water O - acid head group C
0ns
1ns
2ns
3ns
4ns
5ns
6ns
7ns
8ns
g(r)
r (A)
0
0.2
0.4
0.6
0.8
1
0
2
4
6
8
10
12

(d)

Figure 4.3. RDFs for different atom pairs for C3, C8 and C9_branched dicarboxylic acid coated nanoaerosols (a) RDFs of water O-water O (b) RDFs of acid central CH_2-CH_2 groups (c) time evolution of RDFs of acid central CH_2-CH_2 for C3 coated nanoaerosol (d) RDFs of water O-acid head group C for C8 coated nanoaerosol at different equilibration stages

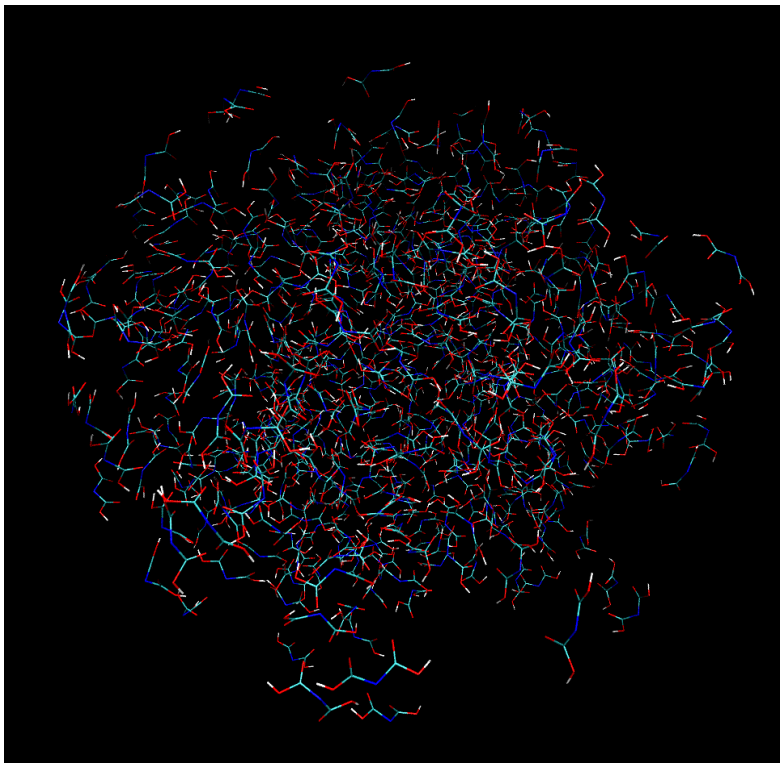

Figure 4.4. Snapshot of C3 acid molecules in the equlibrium phase (For emphasizing, water molecules are removed)

4.4. Phase Separation Mechanism

In order to study the detailed mechanism for phase separation which occurs in long chain dicarboxylic acid coated nanoaerosols, a low surface coverage (10% of the original coverage), C8 coated nanoaerosol was prepared and allowed to evolve from an initial 'inverted micelle' configuration. The images of structure evolution of this nanoaerosol are presented in Figure 4.5.

As can be seen from Figure 4.5, the phase separation process between the acid and water molecules happens in several stages. In the first stage, the C8 acid molecules start to fold on the water droplet surface due to the attraction force between the acid head group and the water molecules (snapshot at 0.1ns). After about 0.5ns of equilibration, all the acid molecules are fully folded and form a uniform layer on the water droplet surface. The next stage of the phase separation process is the aggregation of the acid molecules. As we can see from the snapshot at 1ns, some acid molecules jump on top of other acid molecules and start to form small clusters due to the attraction between the acid molecules. This stage leaves some spaces uncovered on the water droplet surface. At the final stage of the phase separation process, smaller acid clusters attract each other and collide into larger clusters. This leaves even more open spaces on the water droplet surface. The water and acid phases become totally separated.

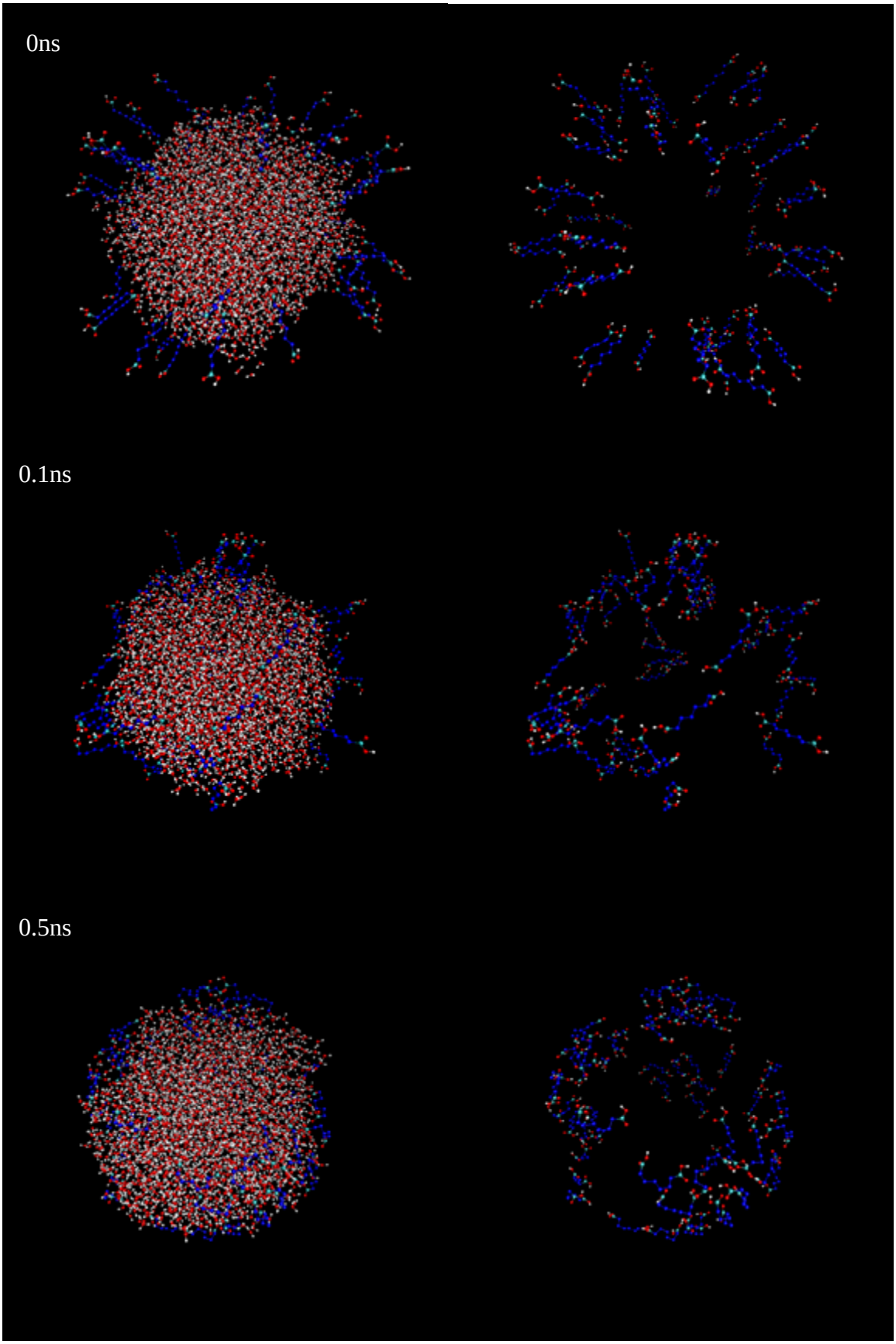
0ns
0.1ns
0.5ns

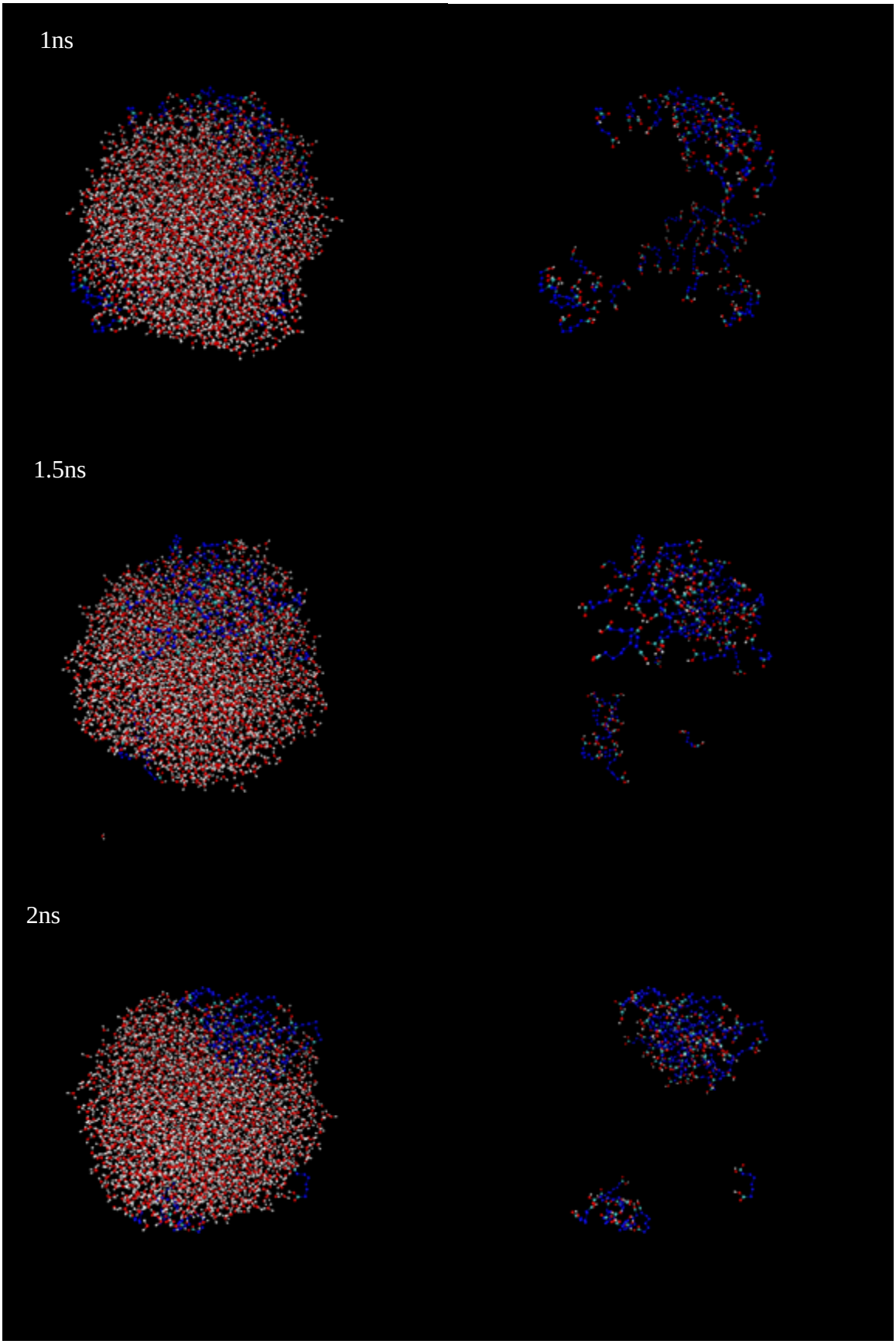
1ns
1.5ns
2ns

Figure 4.5. Phase separation of low coverage C8 acid coated nanoaerosol

4.5. Discussion: Hydrophobicity and the Structure of Dicarboxylic Acid Coated Aqueous Aerosol

The hydrophobic effect is the tendency for non-polar molecules and water to segregate and an important driving force for amphiphlies self-assembly and biological folding[28]. Water makes very strong hydrogen bonding. Each water molecule can participate in four such bonds, sharing its two hydrogen atoms with two neighboring water molecules and sharing two further hydrogen atoms associated with two other neighbors. Mixing enough hydrophobic molecules with water therefore leads to a reduction in favorable bonding. Strong mutual attractions between water molecules induce segregation of non-polar molecules from water and result in an effective attraction between hydrophobic molecules[29]. This water induced attraction is called hydrophobic interaction. When the hydrophobic units are small enough, water molecules can adopt orientations that allow hydrogen-bonding patterns to go around the solute without sacrificing hydrogen bonds. When close to a large hydrophobic object (e.g. an aggregate of small hydrophobic units), the maintaining of a complete hydrogen bond network is geometrically impossible. As a result, water tends to move away from the large hydrophobic object and forms an interface around it[30]. The critical length scale dividing large from small can be estimated to be 1nm[31].

The dicarboxylic acid molecules studied in this work contain a hydrophobic hydrocarbon chain, thus can participate in the hydrophobic interaction with water.

The hydrophilic parts of the dicarboxylic acid molecules are not directly responsible for hydrophobic assemblies, but they can affect the arrangement of these assemblies relative to interfaces and other structures[28]. The structures observed in our simulation for different dicarboxylic acids coated nanoaerosols can be explained successfully using the knowledge of hydrophobic interactions between the acid molecules and the water molecules.

For C3 acid coated nanoaerosol, we observed a final structure with the surface acid molecules totally dissolved into the water and form an ordered cluster structure (see g(r) in Figures 4.3.(b)) at the center of the water droplet. As a result, the original water molecules at the droplet center were excluded, leading to a very low water density at the center region (see Figure 4.2.(a)). This structure is readily understood in terms of the dependence of hydrophobic solvation on the size of hydrophobic unit. When the C3 acid cluster together to form a big hydrophobic unit with a sufficiently large volume to surface ratio that its solvation free energy is lower than the overall salvation free energy of the individual acid molecules. By forming a nearly spherical acid cluster, the total acid surface area exposed to the unfavorable hydrophobic interactions with water is thus minimized. The diameter of this acid cluster is about 2nm which is consistent with the criteria that above 1nm the energetic cost of assembling hydrophobic units is significantly more favorable than the entropic cost of keeping them separate. As discussed above, this hydrophobic interaction also leads to an effective attractive force between acid molecules. With this stronger attractive force than pure van der Waals forces, the acid molecules tend to form an ordered structure.

For nanoaerosols coated with low solubility dicarboxylic acids, we observed phase separation between acid and water at the surface of water droplet with the acid molecules forming a layered aggregate. The radial distribution of the acid aggregate reveals that this aggregate structure is less ordered than the cluster structure formed by C3 acid molecules in water. Since the free energetic cost of dissolving large dicarboxylic acid molecules in water is formidable, the acid molecules will stay on the water droplet surface. However, as we can see from Figure 4.5, due to the two hydrophilic head groups, the first step towards acid molecule aggregation is each individual acid molecule folds on the surface of water droplet with its hydrophilic part attached to water surface. This configuration is not energetically favorable since the hydrocarbon chain in each dicarboxylic acid molecule is close to the water. The equilibration process is to minimize this unfavorable interaction by minimize the total acid surface area exposed to water. Thus, aggregation of acid molecules is the choice. Since this aggregation process happens near the surface of water droplet, the hydrophobic interaction is not as strong as that in the water. Therefore, the final structure of acid aggregate is less ordered than the structure of C3 acid cluster in water.

For the 100% surface coverage C9_branched acid coated nanoaerosol, with the addition of branched chain, the C9_branched acid molecule is hard to fold completely on the water surface due to the geometric constraints. Thus, the hydrophobic part of the acid molecule does not affect by the unfavorable interaction by water. The initial structure of C9_branched acid coated nanoaerosol keeps intact. However, for a low surface coverage C9_branched acid coated nanoaerosol, we do observe the phase

separation between the acid and the water molecules, since in this case the acid molecules can fold on the surface of water droplet. Figure 4.6 compares the configuration of a 100% surface coverage C9_branched acid coated nanoaerosol with the configuration of a 10% surface coverage nanoaerosol after equilibration for 2ns. A phase separation can be clearly seen for the 10% surface covered aerosol.

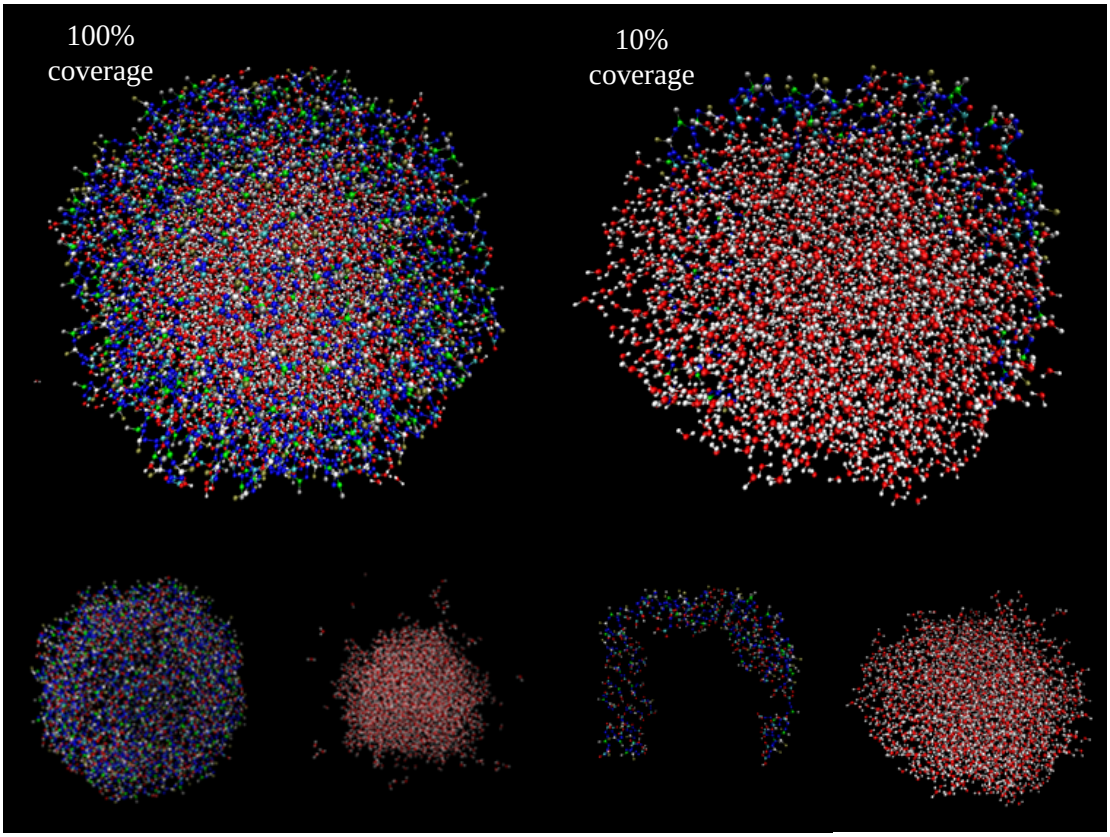

Figure 4.6. Phase separation of 10% surface coverage C9_branched acid coated nanoaerosol

4.6. Diffusion

In order to gain a better understanding of the dicarboxylic acid coating and how it interacts with the water droplet, we computed the diffusion coefficients for the dicarboxylic acid molecules and the water molecules. This is achieved by computing the mean square displacement of the dicarboxylic acid and water molecules in the MD simulation. The diffusion coefficient is evaluated using the following equation:

$$\frac{\partial \left\langle r^2(t) \right\rangle}{\partial t} = 2dD$$

In the above equation, $\left\langle r^2(t) \right\rangle$ is the mean square displacement (MSD) of the molecules being tracked, *t* is time, *d* is the dimension available for diffusion, and D is diffusion coefficient. In our case, it is assumed to be 3. The calculated diffusion coefficients for different dicarboxylic acid molecules are presented in Figure 4.7, in which the acid diffusivity is plotted against the total carbon number in the acid molecules. As can be seen from the figure, the diffusion coefficients of dicarboxylic acid molecules exhibit a general decreasing trend with the total carbon number (molecular size). Except for C3 and C4 molecules which have much larger diffusion coefficients than the other molecules, the diffusion coefficients for C5-C9 molecules follow approximately a linear relationship with the total carbon number. This linearity reflects the linearly increased chain length (size) in acid molecules. The fact that C3 and C4 molecules are more mobile than the other acid molecules suggests a stronger water-acid interaction (hydrophobic interaction). The acid molecules diffuse fast in water medium. The reader is reminded that the C3 acid molecules are fully dissolved

into the water core in the equilibrium structure of C3 coated water droplet while the C4 acid molecules are partially dissolved into the water.

The diffusion coefficients for water molecules in different aerosol structures were also calculated using the Einstein equation. The variation of water diffusivity among different structures is much smaller than that of acid molecules. The average water diffusion coefficient is computed to be 3.45 cm/s^2 at 300K.

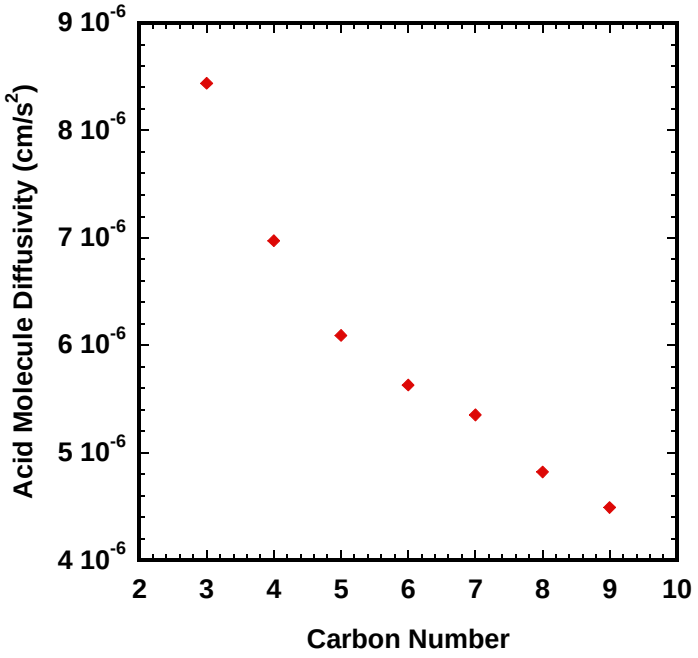

Figure 4.7. Dicarboxylic acid diffusion coefficient as a function of carbon number

Chapter 5: Water Processing of Dicarboxylic Acid Coated Aqueous Nanoaerosol

5.1. Sticking Coefficient

The accommodation of water vapor to liquid water surfaces plays an important role in the growth of cloud condensation nuclei into cloud droplets. Water vapor evaporation from and condensation onto a nanoaerosol are strongly affected by the composition, structure and surface properties of the aerosol. In order to obtain a better understanding of the effect of dicarboxylic acid coating on the aerosol water vapor processing, the water sticking (mass accommodation) coefficient α was calculated for each coated nanoaerosol system. The sticking coefficient describing the probability of gas molecules being incorporated into aerosol is defined as:

$$\alpha = \frac{\text{number of molecules absorbed into the aerosol}}{\text{number of molecules impinging the aerosol surface}}$$

An accurate determination of the water sticking coefficient is important in predicting the nucleation and growth kinetics of cloud droplets.

To compute the water sticking coefficient, we carried out MD simulations in which we placed water monomers outside the aerosol with a random velocity pointing to the aerosol surface and then we calculated the probability of water vapor absorbed into the aerosol.

During each simulation, a single water molecule was placed randomly at a distance of 5nm from the center of the nanoaerosol, outside the potential cutoff distance so that initially no force was acting between the water monomer and the

coated aerosol. The water molecule was then given an initial velocity pointing towards the center of the aerosol which is drawn from the Maxwell-Boltzmann speed distribution at 300K. The trajectory of this water monomer was monitor for 100ps. The water monomer was considered trapped in the aerosol if the distance between the monomer and the coated aerosol is smaller than the size of the aerosol, otherwise, it was considered non-absorbed. More than 60 such water trajectories were computed for each coated aerosol. The water sticking coefficient was then calculated as the ratio of number of absorbed monomers to the number of impinging monomers. The sticking coefficients were calculated for all the structures.

Figure 5.1 presents the results of sticking coefficients calculation for different coated structures. As we can see from Figure 5.1.(a), the water sticking coefficient for C3_coated nanoaerosol is essentially unity at all impinging velocities. The same sticking coefficient result was also found by other researchers studying the water sticking on water surface using MD simulations. For example, Morita et al.[32] studied the mass accommodation (condensation) coefficient α of water vapor into liquid water. The MD scattering simulation predicts $\alpha \sim 1$ at 273 K. Nagayama[33, 34] using two kinds of water intermolecular potentials, the Carravetta-Clementi (C-C) model and the extended simple point charge (SPC/E) model calculated the water condensation coefficients at different temperatures, the result at 330K was 0.961. Thus, our results of water sticking coefficient for C3_coated nanoaerosol is consistent with the fact that the aerosol functions as a pure water droplet for water processing due to the dissolving of acid molecules. Figure 5.1.(b) shows the sticking coefficient calculation results for C9_branched acid coated nanoaerosol. As we can see from the

figure, the sticking coefficient is the largest for incident speed around the most probable speed and smaller at both lower and higher speeds. Compared with pure water droplet, the sticking coefficient for the C9_branched acid coated nanoaerosol is reduced, which indicates that the acid coating impedes the mass transfer from gas phase to the aerosol phase. However, the reduction in the sticking coefficient for the C9_branched acid coated nanoaerosol is not huge, which suggests that even with the insoluble organic coating, the coated aerosol can still process water vapor efficiently.

Due to the phase separation nature of the longer chain dicarboxylic acid coated aerosols, the water impinging simulations are carried out under different conditions. We separated the water trajectories incident onto water phase from the water trajectories incident onto the acid phase. The calculated sticking coefficient for water on water was essentially unity. However, for the water molecules collided onto the acid side, almost all of them reflected back to the gas phase, the sticking coefficient was close to zero. This result is reasonable since the acid molecules formed a thick layered structure, the water molecules were unlike to penetrate this hydrophobic surface.

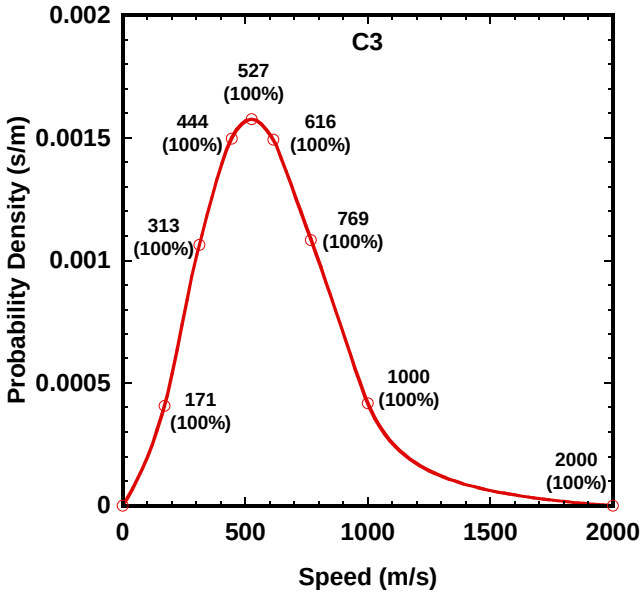

(a)

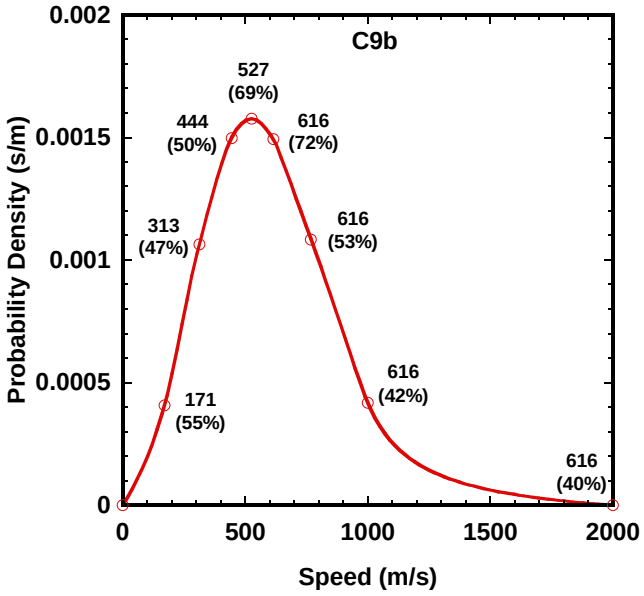

(b)

Figure 5.1. Water vapor sticking coefficient for different coated nanoaerosols (a) C3 acid coated nanoaerosol (b) C9b acid coated nanoaerosol

5.2. Snapshots of Water Collision

In this section, snapshots of water collided on different nanoaerosols are presented in Figure 5.2. For emphasizing, the colliding water molecules are enlarged.

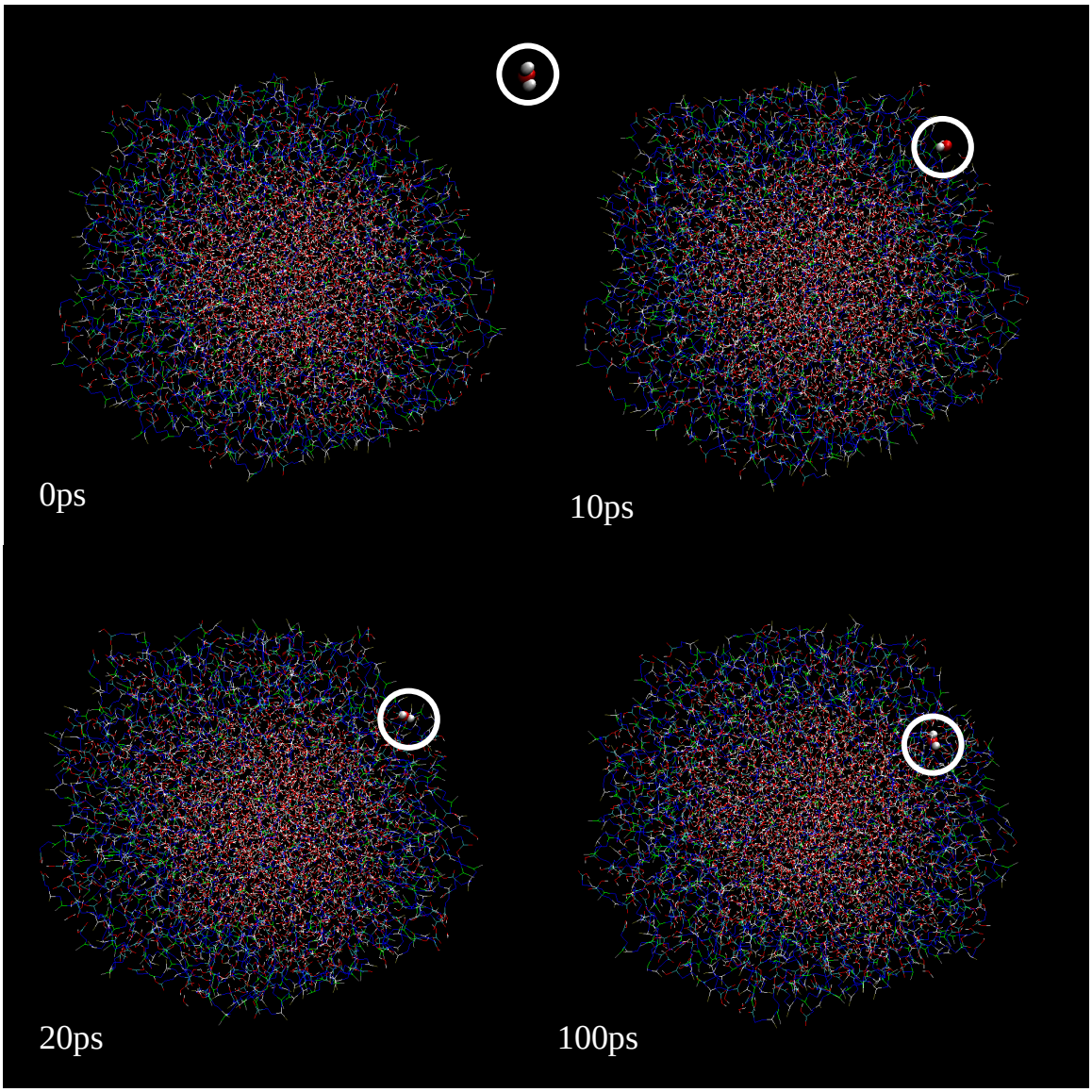

(a) Bonded collision of water on C9_branched acid coated nanoaerosol

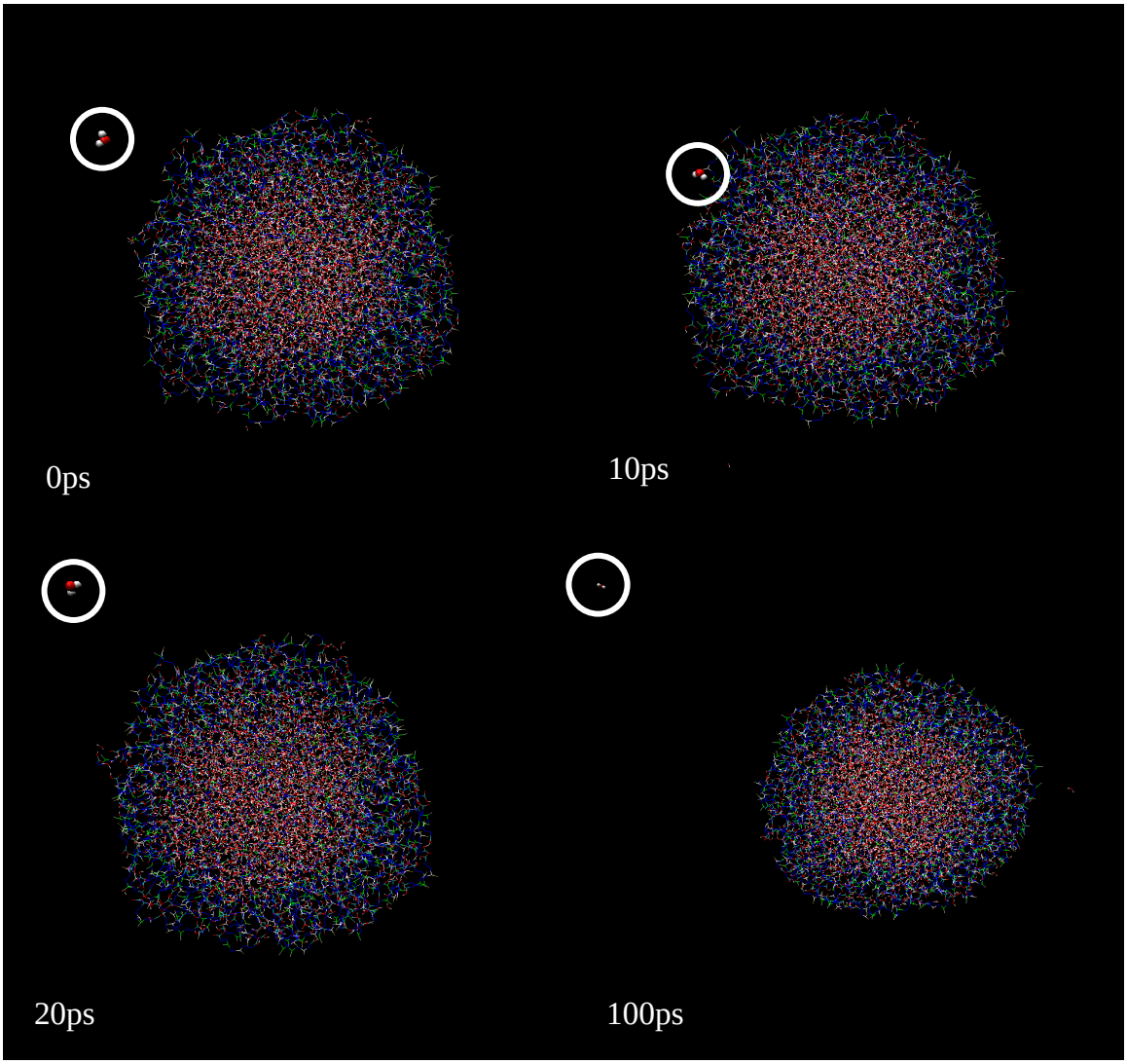

(b) Non-bonded collision of water on C9_branched acid coated nanoaerosol

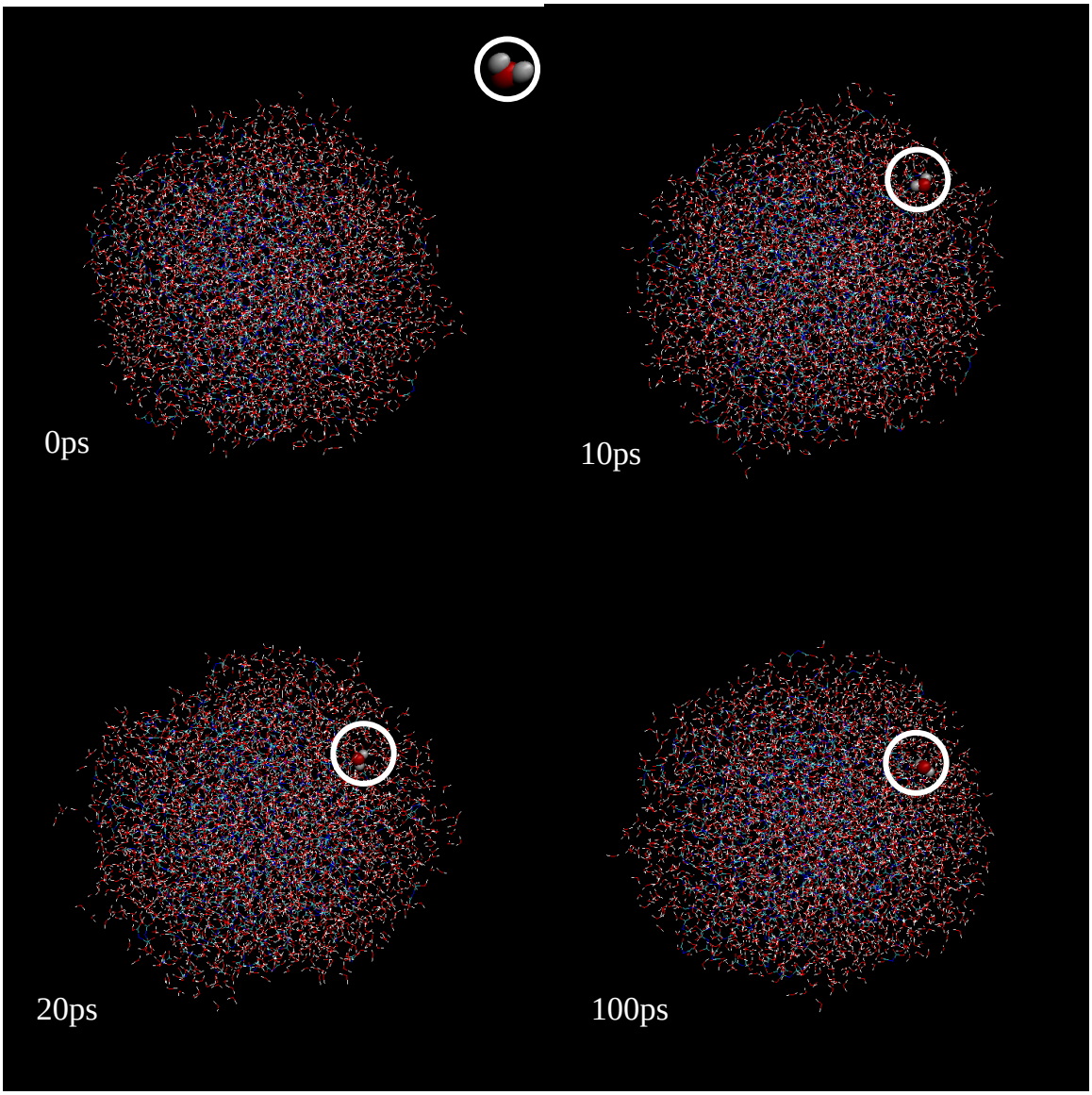

(c) ***Bonded collision of water on C3 acid coated nanoaerosol***

Figure 5.2. Snapshots of water molecule colliding onto different coated nanoaerosols (For emphasizing, the colliding water molecules are enlarged) (a) bonded collision of water on C9_branched acid coated nanoaerosol (b) non-bonded collision of water on C9_branched acid coated nanoaerosol (c) bonded collision of water on C3 acid coated nanoaerosol

Chapter 6: Conclusions and Future Work

6.1. Conclusions

In this work, molecular dynamics simulations were used to probe the structure and the interfacial properties of the dicarboxylic acid coated aqueous aerosol. Low molecular weight dicarboxylic acids of various chain lengths and water solubility (from Malonic acid to Azelaic acid) were chosen to coat a water droplet consisting of 2440 water molecules. The starting point of the coated aerosol is an inverted micelle model. Radial density and radial distribution functions were then obtained and the structure evolutions of the coated aerosols were monitored. For malonic acid coated aerosol, after equilibration, the original surface acid molecules dissolved into the water core. For other nanoaerosols coated with low solubility acids, phase separation between water and acid molecules was observed during the equilibration process. The detailed phase separation mechanism was investigated by monitoring the structure evolution of a 10% surface acid covered nanoaerosol.

To study the water processing of the coated aerosol, the water vapor accommodation factors for the coated aerosols were calculated by bombarding water molecules of certain velocity onto the aerosol. For the C3 acid coated nanoaerosol, a water vapor accommodation factor of 1 was found for all incident water velocities. The whole coated aerosol acts as a bigger water droplet. For longer chain coated nanoaerosols, due to the phase separation, a 100% sticking probability was founded for water monomer colliding onto the water phase of the coated aerosol and an almost 0% sticking probability was founded for water monomer colliding onto the acid phase. For the C9_branched acid coated nanoaerosol, the reduction in sticking

probability is not huge compared with pure water droplet, which suggests that even with the insoluble organic coating, the coated aerosol can still process water vapor efficiently.

6.2. Future Work

Several ideas have been proposed to extend the current work of molecular dynamics simulation of dicarboxylic acid coated aqueous aerosol.

1. Systematically study the effect of surfactant coverage on the structure of coated nanoaerosol.

2. Study the processing of atmospheric organic materials of partially coated nanoaerosol.

3. Study the water processing of these organic coated nanoaerosols by monitoring the changes in equilibrium vapor pressure.

Bibliography

1. Cruz, C. N. & Pandis, S. N. A study of the ability of pure secondary organic aerosol to act as cloud condensation nuclei. Atmospheric Environment 31, 2205-2214 (1997).
2. Shantz, N. C., Leaitch, W. R. & Caffrey, P. F. Effect of organics of low solubility on the growth rate of cloud droplets. Journal of Geophysical Research-Atmospheres 108 (2003).
3. Ervens, B., Feingold, G., Clegg, S. L. & Kreidenweis, S. M. A modeling study of aqueous production of dicarboxylic acids: 2. Implications for cloud microphysics. Journal of Geophysical Research-Atmospheres 109 (2004).
4. Donaldson, D. J., Tervahattu, H., Tuck, A. F. & Vaida, V. Organic aerosols and the origin of life: An hypothesis. Origins of Life and Evolution of the Biosphere 34, 57-67 (2004).
5. Dobson, C. M., Ellison, G. B., Tuck, A. F. & Vaida, V. Atmospheric aerosols as prebiotic chemical reactors. Proceedings of the National Academy of Sciences of the United States of America 97, 11864-11868 (2000).
6. Donaldson, D. J. & Vaida, V. The influence of organic films at the air-aqueous boundary on atmospheric processes. Chemical Reviews 106, 1445-1461 (2006).
7. Chakraborty, P. & Zachariah, M. R. Sticking coefficient and processing of water vapor on organic-coated nanoaerosols. Journal of Physical Chemistry A 112, 966-972 (2008).

8. Ellison, G. B., Tuck, A. F. & Vaida, V. Atmospheric processing of organic aerosols. Journal of Geophysical Research-Atmospheres 104, 11633-11641 (1999).

9. Chakraborty, P. & Zachariah, M. R. "Effective" negative surface tension: A property of coated nanoaerosols relevant to the atmosphere. Journal of Physical Chemistry A 111, 5459-5464 (2007).

10. Hori, M., Ohta, S., Murao, N. & Yamagata, S. Activation capability of water soluble organic substances as CCN. Journal of Aerosol Science 34, 419-448 (2003).

11. Kawamura, K., Semere, R., Imai, Y., Fujii, Y. & Hayashi, M. Water soluble dicarboxylic acids and related compounds in Antarctic aerosols. Journal of Geophysical Research-Atmospheres 101, 18721-18728 (1996).

12. Rozaini, M. Z. H. & Brimblecombe, P. The Odd-Even Behaviour of Dicarboxylic Acids Solubility in the Atmospheric Aerosols. Water Air and Soil Pollution 198, 65-75 (2009).

13. Bilde, M., Svenningsson, B., Monster, J. & Rosenorn, T. Even-odd alternation of evaporation rates and vapor pressures of C3-C9 dicarboxylic acid aerosols. Environmental Science & Technology 37, 1371-1378 (2003).

14. Raymond, T. M. & Pandis, S. N. Cloud activation of single-component organic aerosol particles. Journal of Geophysical Research-Atmospheres 107 (2002).

15. Safran, S. A. Statistical thermodynamics of surfaces, interfaces, and membranes (Addison-Wesley Pub., Reading, Mass., 1994).

16. Fuhrhop, A. H. & Wang, T. Y. Bolaamphiphiles. Chemical Reviews 104, 2901-2937 (2004).

17. Corrigan, C. E. & Novakov, T. Cloud condensation nucleus activity of organic compounds: a laboratory study. Atmospheric Environment 33, 2661-2668 (1999).

18. Haile, J. M. Molecular dynamics simulation (Wiley, New York, 1992).

19. Leach, A. R. Molecular modelling : principles and applications (Prentice Hall, Harlow, England; New York, 2001).

20. Berendsen H C, J. P. M. P., W F van Gunsteren and J Hermans. in Intermolecular Forces (ed. B, P.) 331-342 (The Netherlands, Dordrecht, Reidel, 1981).

21. Berendsen, H. J. C., Grigera, J. R. & Straatsma, T. P. The Missing Term in Effective Pair Potentials. Journal of Physical Chemistry 91, 6269-6271 (1987).

22. Garrett, B. C., Schenter, G. K. & Morita, A. Molecular simulations of the transport of molecules across the liquid/vapor interface of water. Chemical Reviews 106, 1355-1374 (2006).

23. Ryckaert, J. P., Ciccotti, G. & Berendsen, H. J. C. Numerical-Integration of Cartesian Equations of Motion of a System with Constraints - Molecular-Dynamics of N-Alkanes. Journal of Computational Physics 23, 327-341 (1977).

24. Eastwood., R. W. H. a. J. W. Computer simulation using particles (A. Hilger, Bristol [England] ; Philadelphia, 1988).

25. Pollock, E. L. & Glosli, J. Comments on P(3)M, FMM, and the Ewald method for large periodic coulombic systems. Computer Physics Communications 95, 93-110 (1996).

26. Plimpton, S. Fast Parallel Algorithms for Short-Range Molecular-Dynamics. Journal of Computational Physics 117, 1-19 (1995).

27. Wyslouzil, B. E., Wilemski, G., Strey, R., Heath, C. H. & Dieregsweiler, U. Experimental evidence for internal structure in aqueous - organic nanodroplets. Physical Chemistry Chemical Physics 8, 54-57 (2006).

28. Chandler, D. Interfaces and the driving force of hydrophobic assembly. Nature 437, 640-647 (2005).

29. Chandler, D. Hydrophobicity: Two faces of water. Nature 417, 491-491 (2002).

30. Lum, K., Chandler, D. & Weeks, J. D. Hydrophobicity at small and large length scales. Journal of Physical Chemistry B 103, 4570-4577 (1999).

31. Raschke, T. M., Tsai, J. & Levitt, M. Quantification of the hydrophobic interaction by simulations of the aggregation of small hydrophobic solutes in water. Proceedings of the National Academy of Sciences of the United States of America 98, 5965-5969 (2001).

32. Morita, A., Sugiyama, M., Kameda, H., Koda, S. & Hanson, D. R. Mass accommodation coefficient of water: Molecular dynamics simulation and revised analysis of droplet train/flow reactor experiment. Journal of Physical Chemistry B 108, 9111-9120 (2004).

33. Nagayama, G. & Tsuruta, T. A general expression for the condensation coefficient based on transition state theory and molecular dynamics simulation. Journal of Chemical Physics 118, 1392-1399 (2003).

34. Tsuruta, T. & Nagayama, G. Molecular dynamics studies on the condensation coefficient of water. Journal of Physical Chemistry B 108, 1736-1743 (2004).

35. van Duin, A. C. T., Dasgupta, S., Lorant, F. & Goddard, W. A. ReaxFF: A reactive force field for hydrocarbons. Journal of Physical Chemistry A 105, 9396-9409 (2001).

36. Sanz-Navarro, C. F. et al. Molecular dynamics simulations of the interactions between platinum clusters and carbon platelets. Journal of Physical Chemistry A 112, 1392-1402 (2008).

37. van Duin, A. C. T. et al. ReaxFF(SiO) reactive force field for silicon and silicon oxide systems. Journal of Physical Chemistry A 107, 3803-3811 (2003).

38. Strachan, A., van Duin, A. C. T., Chakraborty, D., Dasgupta, S. & Goddard, W. A. Shock waves in high-energy materials: The initial chemical events in nitramine RDX. Physical Review Letters 91 (2003).

39. Raymand, D., van Duin, A. C. T., Baudin, M. & Hermansson, K. A reactive force field (ReaxFF) for zinc oxide. Surface Science 602, 1020-1031 (2008).